Master's Thesis

Analysis on Resistance Changes in Liquid Metal Printed Wires under Strain for Stretchable Applications

Heeyeop Kim

Department of Mechanical Engineering

Ulsan National Institute of Science and Technology

2021

Analysis on Resistance Changes in Liquid Metal Printed Wires under Strain for Stretchable Applications

Heeyeop Kim

Department of Mechanical Engineering

Ulsan National Institute of Science and Technology

Analysis on Resistance Changes in Liquid Metal Printed Wires under Strain for Stretchable Applications

A thesis/dissertation submitted to
Ulsan National Institute of Science and Technology
in partial fulfillment of the
requirements for the degree of
Master of Science

Heeyeop Kim

05.25.2021
Approved by

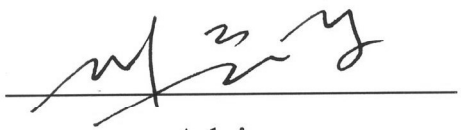

Advisor
Joonbum Bae

Analysis on Resistance Changes in Liquid Metal Printed Wires under Strain for Stretchable Applications

Heeyeop Kim

This certifies that the thesis/dissertation of Heeyeop Kim is approved.

05.25.2021

Signature

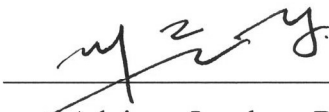

Advisor: Joonbum Bae

Signature

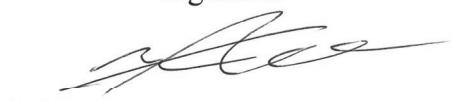

Hooneui Jeong

Signature

Jiyun Kim

Abstract

In the past decade, many studies have been introduced for liquid metal-based stretchable electronics in the form of elastomer silicones embedding liquid metal with various trajectories. However, analyses on the resistance changes in the liquid metal under strain have not been fully exploited yet, which restricted precise estimation of resistance changes under large strain, thus designing the liquid metal-based applications was very challenging to realize the required resistance changes. To overcome these restrictions, in this thesis, relationships between strain and electrical resistance changes in the diagonal and circular arc-shaped wires of liquid metal are analyzed, experimentally verified, and applied to stretchable electronics.

As a first step of the analyses, the resistance changes in diagonal liquid metal wires under strain was formulated with the assumption that the liquid metal wires had no volume change under strain. In addition, by regarding the circular arcs as series of diagonal lines, the resistance changes in circular arc-shaped liquid metal wires under strain was also formulated. Through the tensile tests with fabricated samples in a strain range of 0~150%, the derived formulas were experimentally verified. The result showed that differences between the estimated and measured resistance values were very small, with the root mean square error of less than 0.05.

The derived formulas were applied to stretchable electronics such as a strain sensor and a stretchable heater. The strain sensor including semicircular wires needed to be more accurately estimated for its resistance changes under strain, and the stretchable heater needed to keep its temperature constant under strain. Through the tests, it was proved that the resistance changes in the applications were accurately estimated and realized as required, which verified that the derived formulas are applicable to real stretchable electronics.

Contents

List of Figures

List of Tables

Chapter 1. Introduction

The wearable device market has rapidly grown nowadays, and is expected to be more increased in the future as shown in Figure 1.1 [1, 2]. With these expectations, numerous studies have presented stretchable electronics, consisting of a silicone elastomer and electrical conductors including carbon nanotubes, metal-based nanowires, and liquid metals as shown in Figure 1.2 [3-14]. Among the electrical conductors, eutectic gallium-indium (eGaIn), one of the gallium-based liquid metals shows superior characteristics such as low toxicity, high electrical and thermal conductivity [15]. Thus, eGaIn has been adopted as a material for electrical wires in stretchable electronics. In addition, even though eGaIn is liquid state at room temperature by its low melting point of 15.5 ℃ [16], eGaIn keeps its shape in virtue of the oxide layer on its surface [17]. This specificity allows direct ink writing, a way to directly draw electrical conductors on the elastomer, and leads to flexible patterning of eGaIn wires [18].

[1]

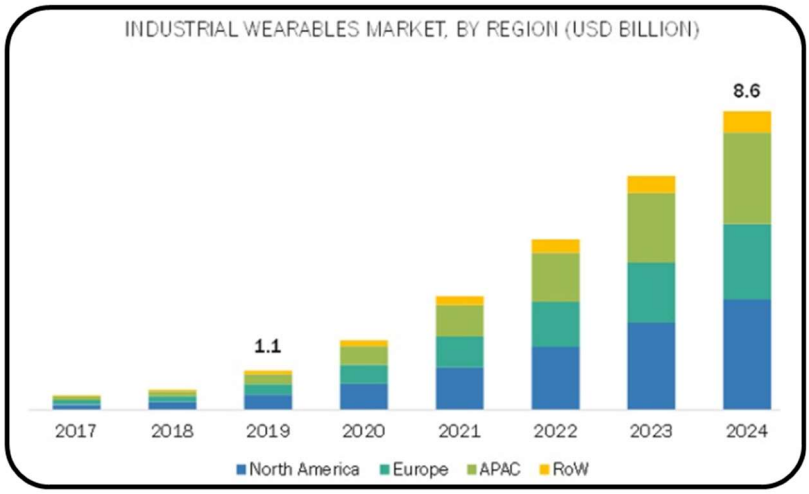

[2]

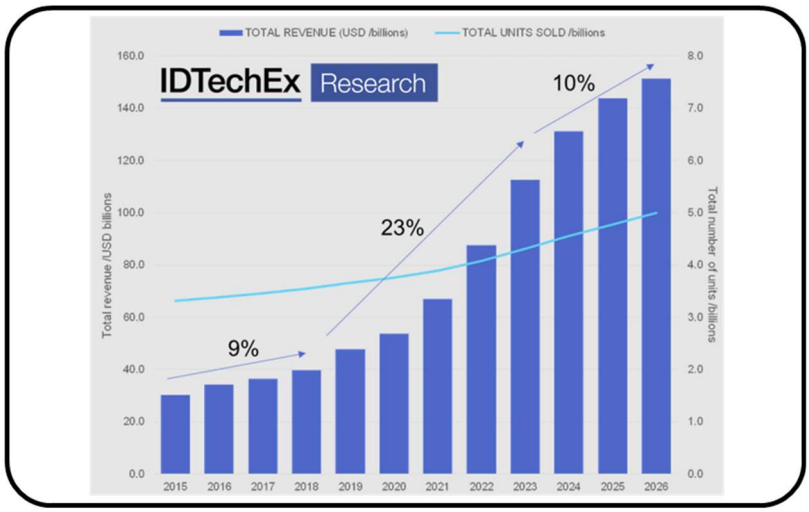

Figure 1.1 Growth of the wearable device market [1, 2]

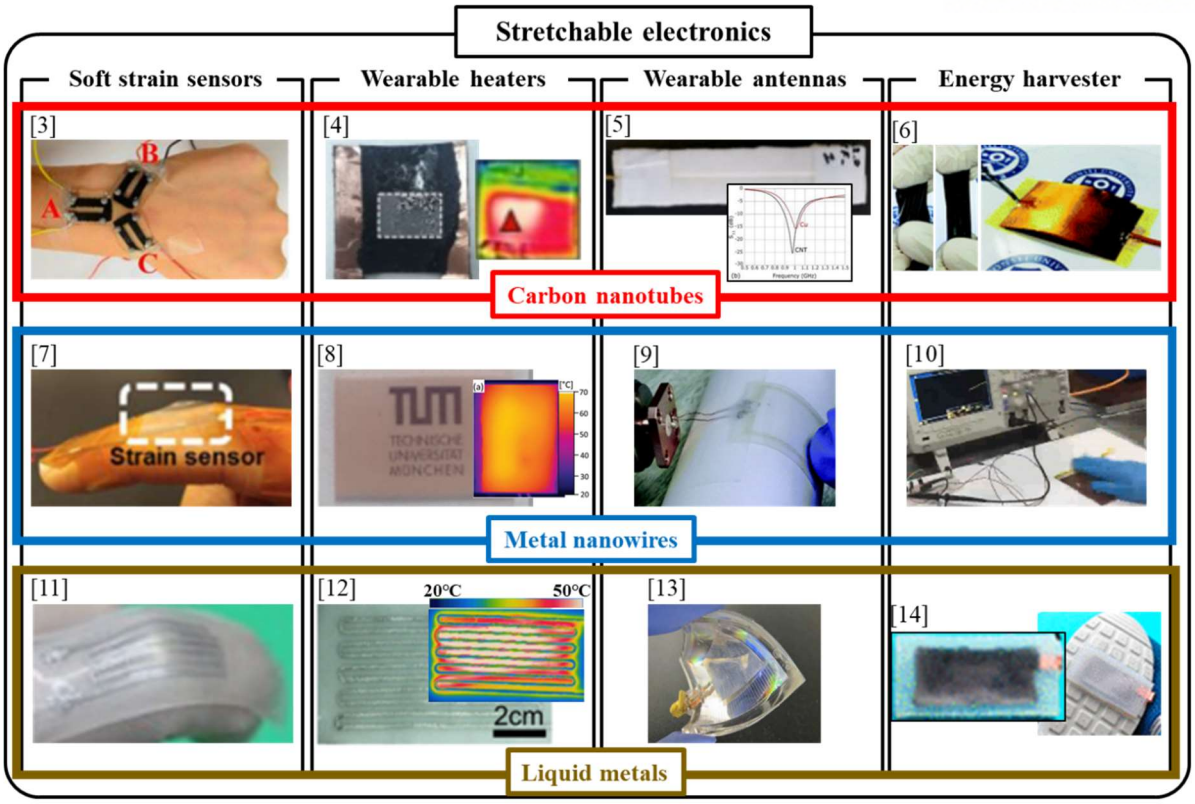

Figure 1.2 Recent studies on stretchable electronics [3-14]

When eGaIn is used as electrical wires, the eGaIn wires embedded in elastomer are dominantly affected by the consistent deformation of the hyper-elastic elastomer [19]. It results that the eGaIn wires have more regular changes in the electrical resistance during repeated strain than other electrical wires based on solid conductors such as carbon nanotubes (CNTs) and metal nanowires (metal-NWs) as shown in Figures 1.3 and 1.4, because of random changes in positions of the solid conductors for each strain [18, 20-22].

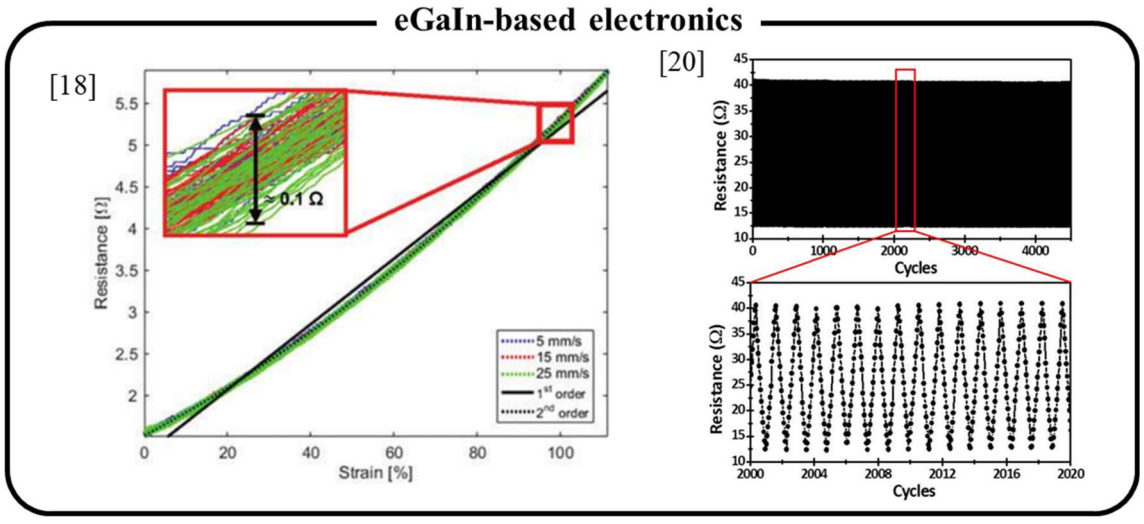

Figure 1.3 Resistance changes in eGaIn wires during repeated strain [18, 20]

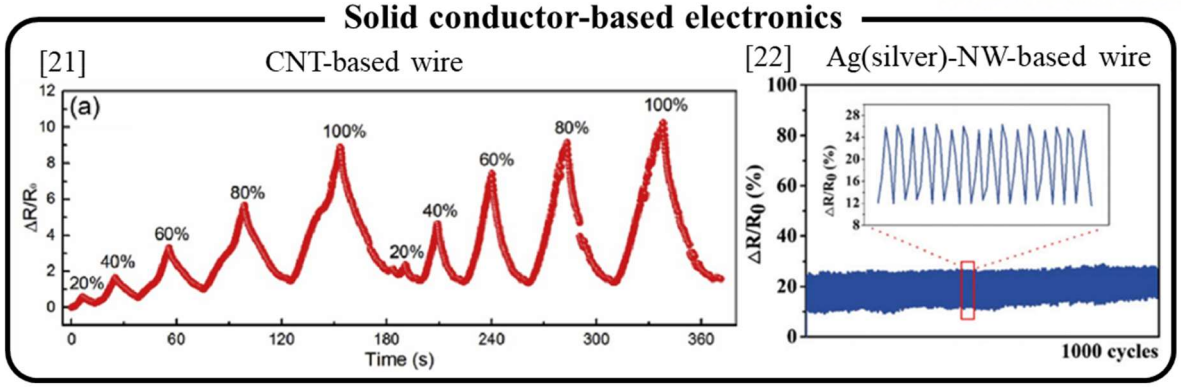

Figure 1.4 Resistance changes in CNT and Ag-NW-based wires during repeated strain [21, 22]

The electrical regularity of the eGaIn wire under repeated strain serves as a great advantage for stretchable applications that is premised on repetitive use, and has influenced increasing interests in studies on eGaIn-based stretchable electronics [18, 20, 23-29, 35, 71, 72]. During the introduction of a variety of eGaIn applications, various shapes of eGaIn trajectories have been also presented to realize the required resistance changes under strain. However, the lack of the physical understanding of the complex trajectories under strain has led to no precise validation on whether the resistance changes in the eGaIn applications were theoretically reasonable. Some studies have presented the physical interpretation of simple trajectories such as tensile directional and tensile-vertical eGaIn wires under strain, but it has not been sufficient to understand eGaIn applications with complicated trajectories such as diagonal or curved trajectories [20, 27, 35].

In the case of eGaIn-based strain sensors, curved wires were included in their trajectories but neglected, causing the possibility of unexpected errors. Estimation of the resistance changes in the sensors under strain is important because the resistance change means the sensitivity, which is the main performance of the sensors. For the accurate estimation, the eGaIn wires in the sensors are separated into stationary and stretchable parts. The stretchable wires are arranged as long as possible in the tensile direction to maximize the resistance change, while the stationary eGaIn wires, which are grabbed and fixed when stretch, have no resistance changes so are required to be relatively short. Generally, the tensile directional eGaIn wires were placed in parallel and connected by semicircular wires as shown in Figure 1.5 (orange line boxes) [18, 24]. However, in previous studies [18, 23, 24], the resistance changes in eGaIn sensors have been estimated with the assumption that the entire wire is tensile directional, which caused the dissimilarity between the estimated and actual resistance change of the sensors.

Especially, a critical problem caused by the ignorance of the semicircular wires occurs when the applied strain becomes much larger; with the large strain, the estimation errors significantly increase due to the growing difference in deformation between the tensile directional and semicircular wires. Given that some studies have presented eGaIn applications with a stretchability of over 500 % [25, 71, 72], and one of them [25] has used a curve-patterned eGaIn wire, the analysis for the semicircular wires is required for the precise estimation of the resistance changes under large strain.

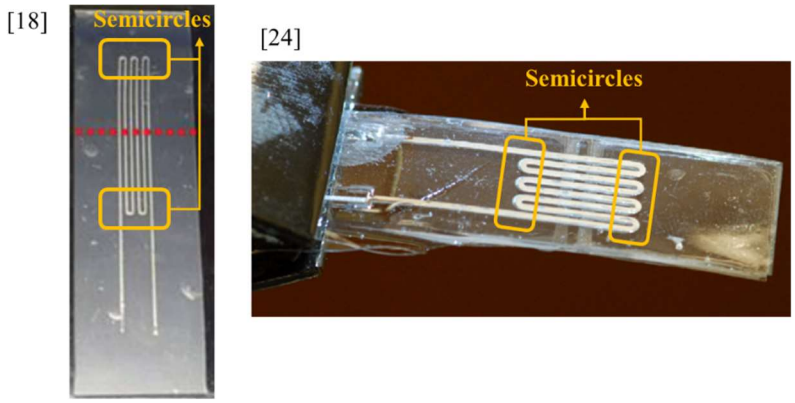

Figure 1.5 eGaIn-based strain sensors with semicircular eGaIn wires (orange line boxes) [18, 24]

Furthermore, complicated eGaIn trajectories may be required for other eGaIn applications such as stretchable heaters. The eGaIn heaters, which adopt the stretchability of eGaIn and an elastomer silicone, transmit the heat generated by electrical current passing through the resistance of eGaIn wires. Here, the acquisition of both stretchability and heat generation triggers a challenging issue: when the eGaIn heaters are under strain, changes in heating power are followed by the resistance changes, as implied in the equation of electrical power, $P=V^2/R$, where P is the electrical power for heating, V is the voltage applied to the heater, and R is the resistance of the heater. Considering an expansion of a heating area in the strained eGaIn heater, increased electrical power is required to let the heater heat up with a constant temperature under strain [25, 26] (Figure 1.6). Accordingly, the resistance of the eGaIn heater is required to decrease under strain, if the applied voltage is uniform.

Some studies have attempted to reduce changes in resistance and temperature of eGaIn heaters under strain by using mixtures of eGaIn and other materials as heating wires (Figure 1.7) [27-29]. However, this approach reaches another limit; it is hard to maintain not only temperature but also resistance of the mixture-based wires constant under strain. Interestingly, the tensile-vertical eGaIn wire has the decreased resistance under strain [30] but the degree of their resistance reduction cannot be adjusted, which makes it impossible to realize the desired resistance change. As an alternative, the eGaIn wires tilted almost vertically can make the adjustability in resistance reduction so can be adopted for the heater having a constant heating temperature.

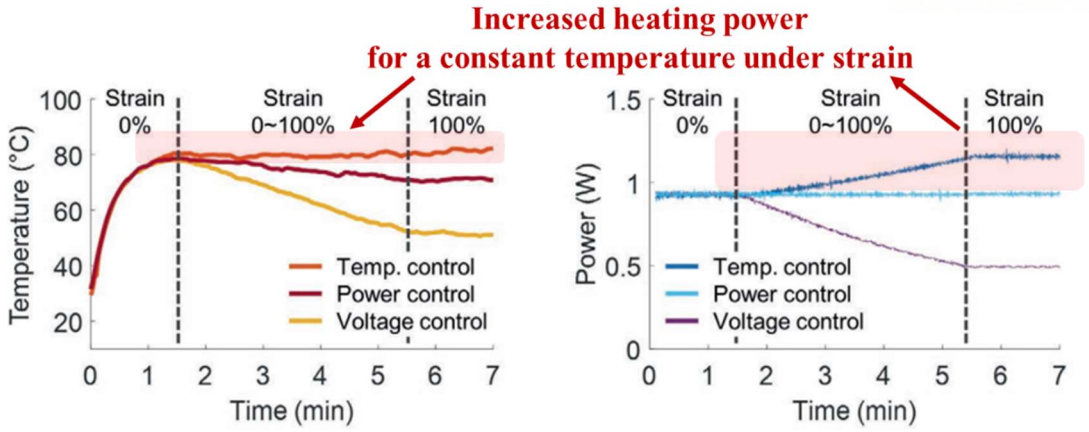

Figure 1.6 Increased heating power required for a constant temperature under strain [26]

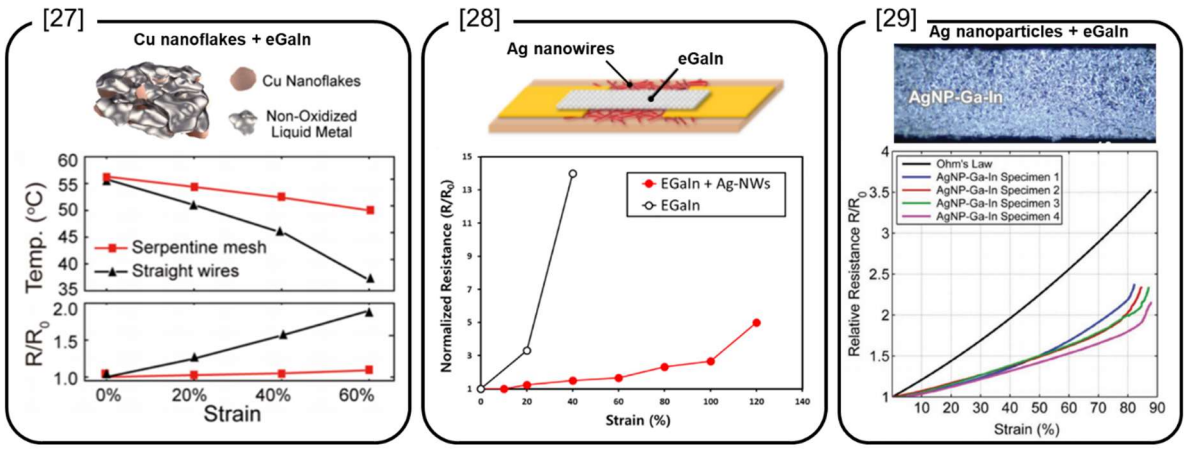

Figure 1.7 Reduced changes in resistance of eGaIn-mixture-based wires under strain [27-29]

The issues of the eGaIn strain sensors and heaters have a common point that analyses on the resistance changes in complicated eGaIn trajectories under strain are needed. In response, the resistance changes in diagonal and circular arc-shaped eGaIn wires under strain were formulized, verified, and applied to stretchable electronics in this thesis.

The remainder of this thesis is organized as follows. In Chapter 2, relationships between the applied uniaxial strain and resistance changes in eGaIn wires patterned by diagonal lines and circular arcs are formalized. The formalized resistance estimation models are verified with tensile tests in Chapter 3. In Chapter 4, the verified resistance estimation models are applied to eGaIn-based electronics. Lastly, the conclusion and open issues are summarized in Chapter 5.

Chapter 2. Formulation of resistance estimation models

2.1 Assumptions for simplifying Pouillet's law

2.1.1 Pouillet's law

Let's assume we have an electrical wire as shown in Figure 2.1. The resistance values of the wire can be expressed by Pouillet's law [31], which defines the relationship between electrical resistance (R), resistivity (ρ), length (L), and cross-sectional area (A) of the wire as follows:

$$R = \rho \frac{L}{A} \tag{2.1}$$

Pouillet's law also can be applied to the electrical wire consisting of eGaIn. If the eGaIn wire is strained, resistance changes in the eGaIn wire can be expressed by the normalized resistance as follows (2.2), where subscript 0 means the initial state without strain:

$$\frac{R}{R_0} = \frac{\rho \frac{L}{A}}{\rho_0 \frac{L_0}{A_0}} \tag{2.2}$$

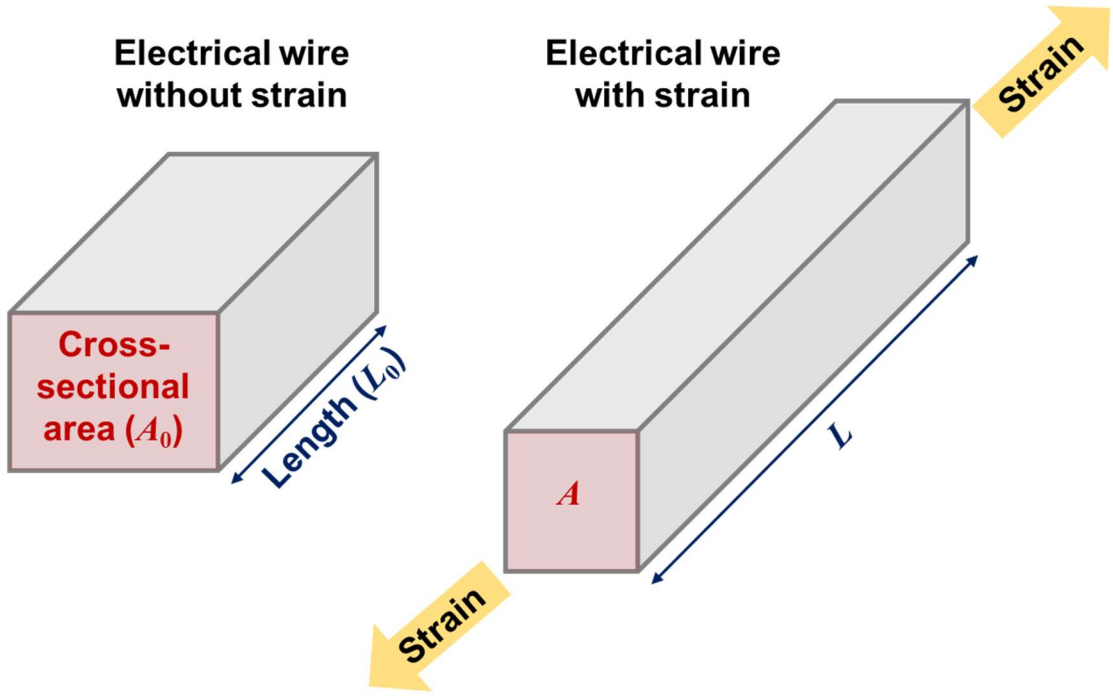

Figure 2.1 Electrical wires with and without strain

2.1.2 Assumptions

Due to no chemical and thermal change, the electrical resistivity of eGaIn is constant under strain regardless of the applied strain. Thus, the resistance change in the eGaIn wire can be modified as follows:

$$\frac{R}{R_0} = \frac{L}{L_0} \times \frac{A_0}{A} \tag{2.3}$$

Here, additional assumptions are established; 1) the eGaIn wire has no resistive force to deformation of elastomer during strain, 2) the elastomer, one of the rubber-like materials regarded to be isotropic and iso-volumetric [32], has dominant effects on deformation of the eGaIn wire, and 3) the internal stress triggered by strain is uniform in cross-sectional areas of the entire elastomer. With these assumptions, the eGaIn wire goes through no volume change and no stress concentration. Thus, the value multiplied by the length and cross-sectional area of the eGaIn wires is unchanged under strain and expressed as follows:

$$LA = L_0 A_0 \tag{2.4}$$

The assumed iso-volumetry of the elastomer modifies the equation on the resistance change in the eGaIn wire as follows:

$$\frac{R}{R_0} = \left(\frac{L}{L_0}\right)^2 \tag{2.5}$$

It is interesting that the aforementioned assumptions include no restriction on a trajectory or cross-sectional shape of the eGaIn wire. That is, as long as the elastomer embedding the eGaIn wire is iso-volumetric, the normalized resistance of the eGaIn wire is equal to the square of the normalized length, regardless of the shape of the eGaIn wire. This gives a chance to analyze resistance changes in eGaIn wires of various trajectories.

2.2 Relationship between resistance and uniaxial strain

2.2.1 Tensile directional eGaIn wire

Under uniaxial strain (ε), the length of a tensile directional eGaIn wire increases, as shown in Figure 2.2. Thus, the resistance change in a tensile directional eGaIn wire is expressed as follows:

$$\frac{R}{R_0} = (1+\varepsilon)^2 \tag{2.6}$$

Equation (2.6), the resistance changes in a tensile directional eGaIn wire under strain, has been used constantly by most existing studies that try to present theoretical changes in resistance under strain [18, 23- 25, 30, 33], but is not appropriate at all if the eGaIn wire is not arranged in the tensile direction.

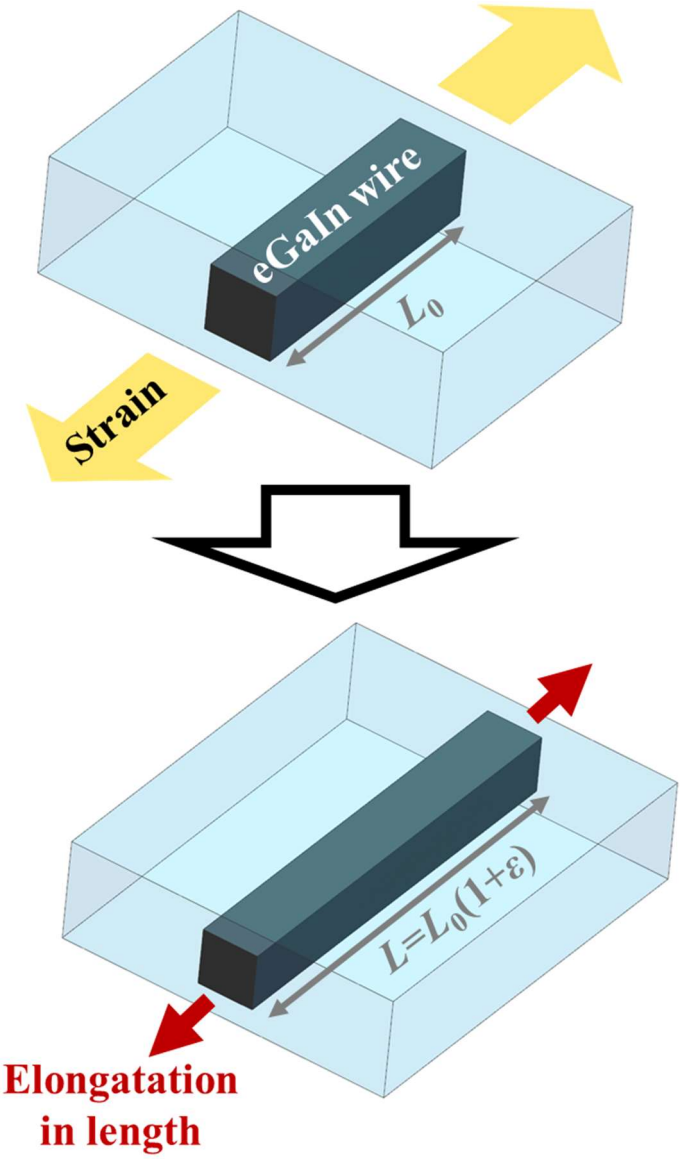

Figure 2.2 Tensile directional eGaIn wires with and without strain

2.2.2 Tensile-vertical eGaIn wire

Some studies have attempted to propose the resistance changes in a tensile-vertical eGaIn wire under strain [30, 33]. As shown in Figure 2.3, when a tensile-vertical eGaIn wire is under strain, the applied strain plays a role to shorten the length of the eGaIn wire, and the iso-volumetry of the elastomer makes this length shrinkage simple as follows:

$$\frac{R}{R_0} = \frac{1}{1+\varepsilon} \tag{2.7}$$

For a more detailed explanation, a rectangle with a length of L, a width of W, the height of H, and the volume of V is assumed to be under strain. Then, the deformation of the rectangle under strain is expressed with Poisson's ratio (v) as follows:

$$\frac{V}{V_0} = (1+\varepsilon)(1-v\varepsilon)^2 = 1 \tag{2.8}$$

Equation (2.8) implies that changes in the width and height of the rectangle can be expressed by only the applied strain as following equation (2.9). Given that, under strain, the lateral deformation of a tensile directional eGaIn wire is the same as the longitudinal deformation of a tensile-vertical eGaIn wire, it makes sense that equation (2.7) shows the square of equation (2.9).

$$\frac{W}{W_0} = \frac{H}{H_0} = 1 - v\varepsilon = \frac{1}{\sqrt{1+\varepsilon}} \tag{2.9}$$

In addition, under strain, a tensile directional eGaIn wire have an increased resistance because the applied strain elongates the length of the eGaIn wire, while a tensile-vertical eGaIn wire have a decreased resistance due to the enlargement of its cross-sectional area by stretch of the width of the eGaIn wire. These increased and decreased resistances in the tensile directional and tensile-vertical eGaIn wires are mathematically described in equations (2.6) and (2.7), respectively.

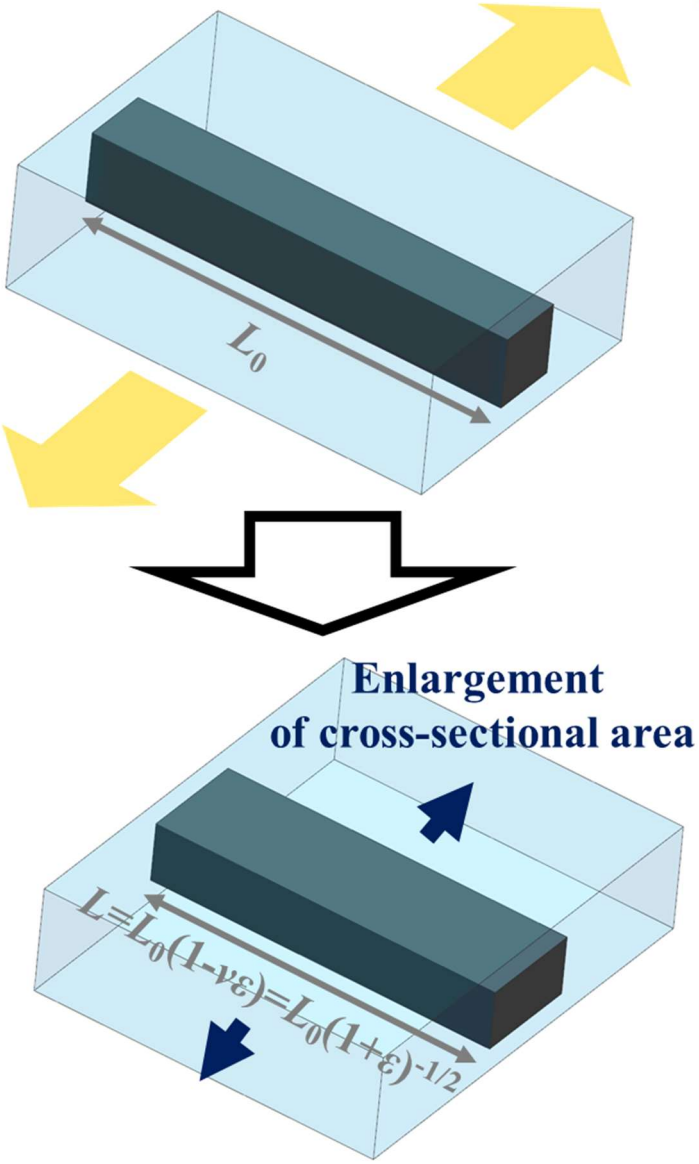

Figure 2.3 Tensile-vertical eGaIn wires with and without strain

2.2.3 Diagonal eGaIn wire

Although the derived equation on the change in resistance of a tensile-vertical eGaIn wire under strain provides possibilities for more varied eGaIn wire patterns to be considered, it is still not applicable to estimation on resistance changes in diagonal or arc-shaped eGaIn wires [21, 35, 36]. In order to break through this restriction, the relationship between strain and resistance changes in a diagonal eGaIn wire, whose initial lengths along the tensile direction and the tensile-vertical direction are respectively *a* and *b* (Figure 2.4), is formalized. Considering its length change under strain, the resistance change in the diagonal eGaIn wire under strain is expressed as follows:

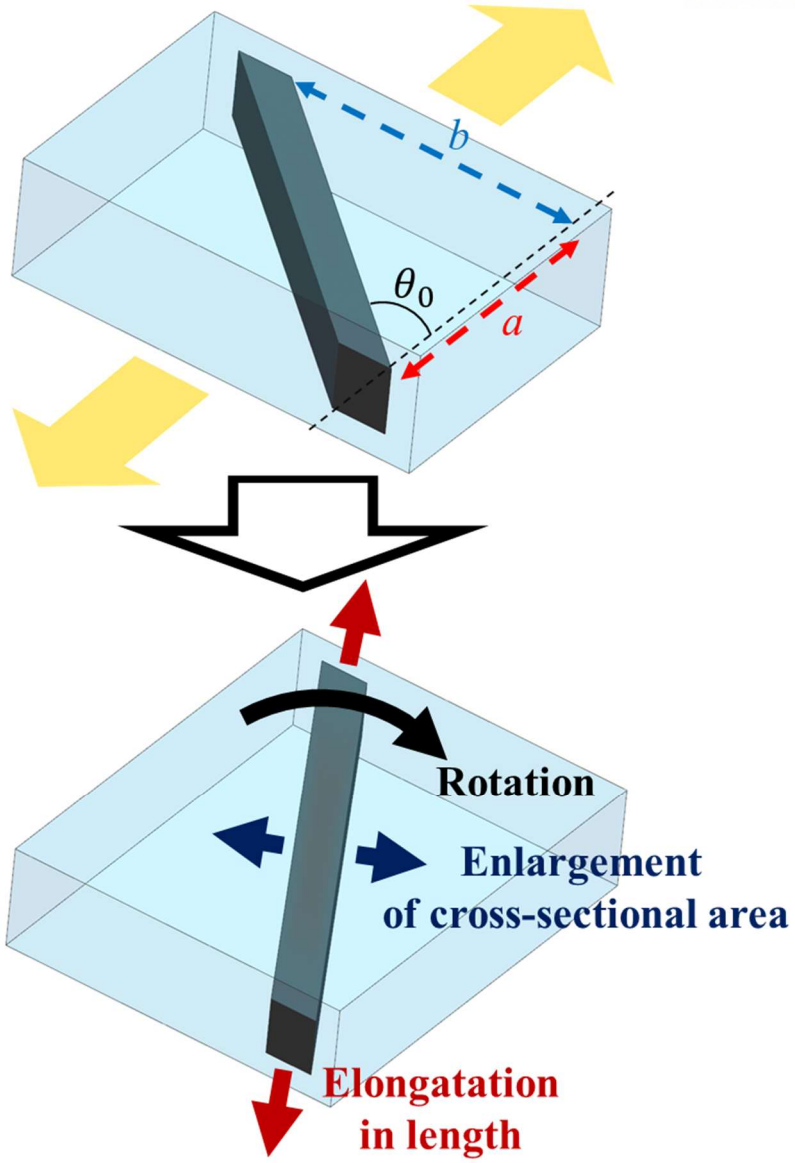

Figure 2.4 Diagonal eGaIn wires with and without strain

$$\frac{L}{L_0} = \frac{\sqrt{a^2(1+\varepsilon)^2 + \frac{b^2}{1+\varepsilon}}}{\sqrt{a^2+b^2}} \tag{2.8}$$

Unlike the tensile directional and tensile-vertical eGaIn wires, resistance changes in a diagonal eGaIn wire under strain are affected by its rotation, as shown in Figure 2.4. All eGaIn wires presented in this thesis were drawn and strained on a two-dimensional plane, thus, diagonal eGaIn wires have verticality relative to the tensile direction as the form of two-dimensional tilt angles (θ), which are changed by the applied strain as follows:

$$\tan\theta = \frac{b}{a(1+\varepsilon)^{3/2}} \tag{2.9}$$

The tangent of an initial tilt angle becomes b/a as follows (2.10) and b/a, employed as a parameter to determine the verticality of a diagonal eGaIn wire, is named 'the verticality' hereinafter.

$$\tan\theta_0 = \frac{b}{a} \tag{2.10}$$

Now, in consideration of the length change in a diagonal eGaIn wire under strain and the initial tilt angle, the resistance change in the diagonal eGaIn wire under strain can be derived as follows:

$$\frac{R}{R_0} = \frac{1}{2(1+\varepsilon)}\left((1+\varepsilon)^3 + 1 + \left((1+\varepsilon)^3 - 1\right)\cos 2\theta_0\right) \tag{2.11}$$

As shown in Figure 2.4, the diagonal eGaIn wire under strain experiences rotation, elongation in the length, and enlargement in the cross-sectional area, which are respectively relevant to a cosine term, numerator terms, and denominator terms in equation (2.11). Under strain, the rotation, decided by the initial tilt angle, has effects on the resistance changes by giving varieties to the ratio between elongation in the length and enlargement in the cross-sectional area, as suggested by the fact that coefficient of the cosine term, i.e., $\left((1+\varepsilon)^3 - 1\right)/2(1+\varepsilon)^3$, is affected by the initial tilt angle in equation (2.11). Namely, the resistance change in the diagonal eGaIn wire under strain can be adjusted by the initial tilt angle, or the verticality. For instance, when the initial tilt angle becomes 0° or 90°, the whole of rotation switches to elongation in the length or enlargement in the cross-sectional area, respectively, and the change in resistance of a diagonal eGaIn wire turns into the change in that of the tensile directional eGaIn wire or tensile-vertical eGaIn wire, respectively.

2.2.4 Circular arc-shaped eGaIn wire

The resistance changes in a circular arc-shaped eGaIn wire under strain is also predictable if the circular arc is considered as a sequence of countless tiny diagonal lines. Let us assume that a circular arc-shaped eGaIn wire has a starting angle of λ_s and an ending angle of λ_e between an angle range of 0~90°. The arc eGaIn wire can be segmented into a total of n diagonal eGaIn wires having equal length, as shown in Figure 2.5. Then, the central angle of the arc eGaIn wire is divided equally as follows:

$$\Delta\lambda = \frac{\lambda_e - \lambda_s}{n} \tag{2.12}$$

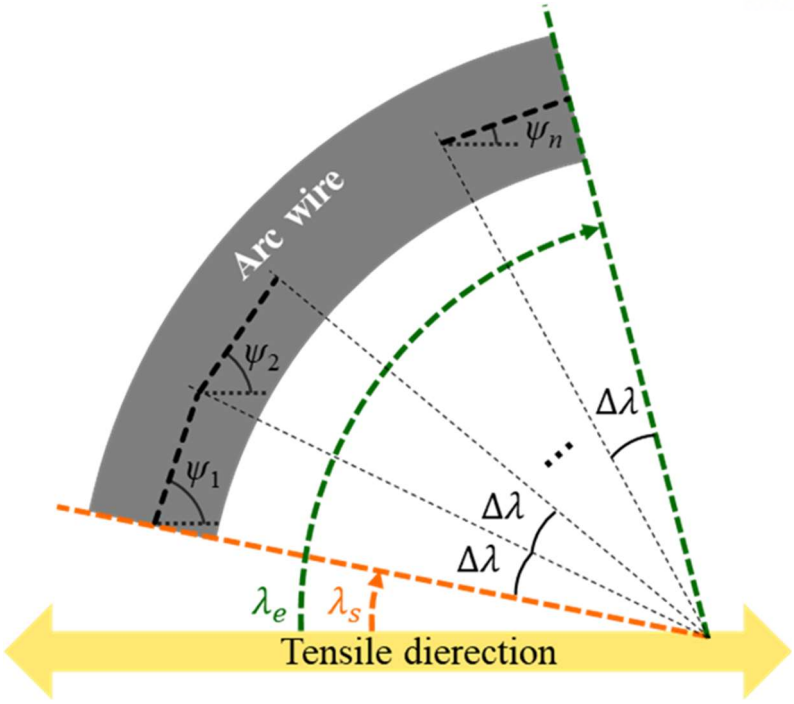

Figure 2.5 Top view of a circular arc-shaped eGaIn wire

Here, the *j*-th diagonal eGaIn wire segment has the tilt angle (ψ_j) that is expressed with the divided central angle ($\Delta\lambda$) as follows:

$$\psi_j = \frac{\pi}{2} - \lambda_s - \frac{1}{2}(1+2j)\Delta\lambda \tag{2.13}$$

By taking into account the tilt angle, the resistance change in the *j*-th diagonal eGaIn wire segment under strain is expressed as follows:

$$\left(\frac{R}{R_0}\right)_j = \frac{1}{2(1+\varepsilon)}\left((1+\varepsilon)^3 + 1 + \left((1+\varepsilon)^3 - 1\right)\cos 2\psi_j\right) \tag{2.14}$$

The diagonal eGaIn wire segments have equal effects on the resistance change in the entire arc eGaIn wire due to their same length, so, the resistance changes in the diagonal eGaIn wire segments under strain are divided by *n* for derivation of the resistance changes in the arc eGaIn wire under strain. In addition, if the lengths of the diagonal eGaIn wire segments come to be tiny, the sequence of diagonal eGaIn wire segments will become considerably analogous to an arc eGaIn wire. Taken together, the resistance change in the arc eGaIn wire under strain can be mathematically expressed by the summation of the resistance change in the *j*-th diagonal eGaIn wire segments under strain, which are divided by *n*, from $j = 1 \ldots n$, as *n* approaches infinity, as follows:

$$\frac{R}{R_0} = \lim_{n\to\infty}\left\{\sum_{j=1}^{n}\left[\frac{1}{2n(1+\varepsilon)}\left((1+\varepsilon)^3+1+\left((1+\varepsilon)^3-1\right)\cos 2\psi_j\right)\right]\right\} \tag{2.15}$$

Equation (2.15) is computed and becomes as follows:

$$\frac{R}{R_0} = \frac{1}{2(1+\varepsilon)}\left((1+\varepsilon)^3+1-\left((1+\varepsilon)^3-1\right)\frac{\sin(\lambda_e-\lambda_s)\cos(\lambda_e+\lambda_s)}{\lambda_e-\lambda_s}\right) \tag{2.16}$$

It is reasonable that the resistance estimation model for the circular arc-shaped eGaIn wire, equation (2.16), is analogous to that for the diagonal eGaIn wire, equation (2.11), because a circular arc is assumed to be a sequence of diagonal lines during the derivation of equation (2.16). Only one dissimilarity between equations (2.11) and (2.16) is the way to describe the rotation of the eGaIn wire: $\cos 2\theta_0$ for a diagonal eGaIn wire in equation (2.11) but $\sin(\lambda_e-\lambda_s)\cos(\lambda_e+\lambda_s)/\lambda_e-\lambda_s$ for a circular arc eGaIn wire in equation (2.16). This dissimilarity explains that the rotation and resistance change in an eGaIn wire are determined by its trajectory shape, and ultimately, it gives an apparent explanation on the reason why the resistance change in a diagonal eGaIn wire and a circular arc-shaped eGaIn wire can be adjusted by the tilt angle and the starting or ending angle. Another interesting point is that when the starting angle is approximated to the ending angle, $\sin(\lambda_e-\lambda_s)/\lambda_e-\lambda_s$ becomes 1 and the resistance estimation model for the circular arc-shaped eGaIn wire turns into that for the diagonal eGaIn wire, whose tilt angle is $90°-\lambda_s$ due to the 90° difference between the starting angle of the circular arc-shaped eGaIn wire and the tilt angle of the diagonal eGaIn wire segment, as suggested in the tilt angle of a diagonal eGaIn wire segment, equation (2.13). Consequently, no theoretical defect is found in the derived resistance estimation models.

Chapter 3. Verification of the estimation models

3.1 Experimental setup for tensile tests

3.1.1 Fabrication of verification samples

Even if no doubt is placed in the logical validity of the derived resistance estimation models for the diagonal and circular arc-shaped eGaIn wires, experimental proofs must be accompanied for practical applications. In order to verify the estimation models, resistance values of samples consisting of an elastomer matrix and eGaIn are required to be measured under strain. Therefore, the fabrication of samples is the first step of the verification.

The verification samples were fabricated with eGaIn [36] and Solaris [37], one of the silicone elastomers, in accordance with the process shown in Figure 3.1. Firstly, uncured Solaris was spread thinly on a silicon wafer by using a film applicator [38] and cured in a heating oven [39] at 60℃ for 30 minutes. Next, the eGaIn wire was drawn on the cured Solaris layer by means of the direct ink writing with the use of a 3-axis dispenser [40]. Uncured Solaris was again spread by the film applicator for encapsulation of the drawn eGaIn wires and cured in the heating oven again. The cured Solaris was trimmed by hand with a scalpel [41, 42]. Lastly, copper wires were put into the eGaIn wires and bonded to the Solaris by a silicone adhesive [43]. The silicone adhesive was cured in a heating oven at 120℃ for 10 minutes. All of the fabricated sampled in this thesis were about 0.8 mm thick.

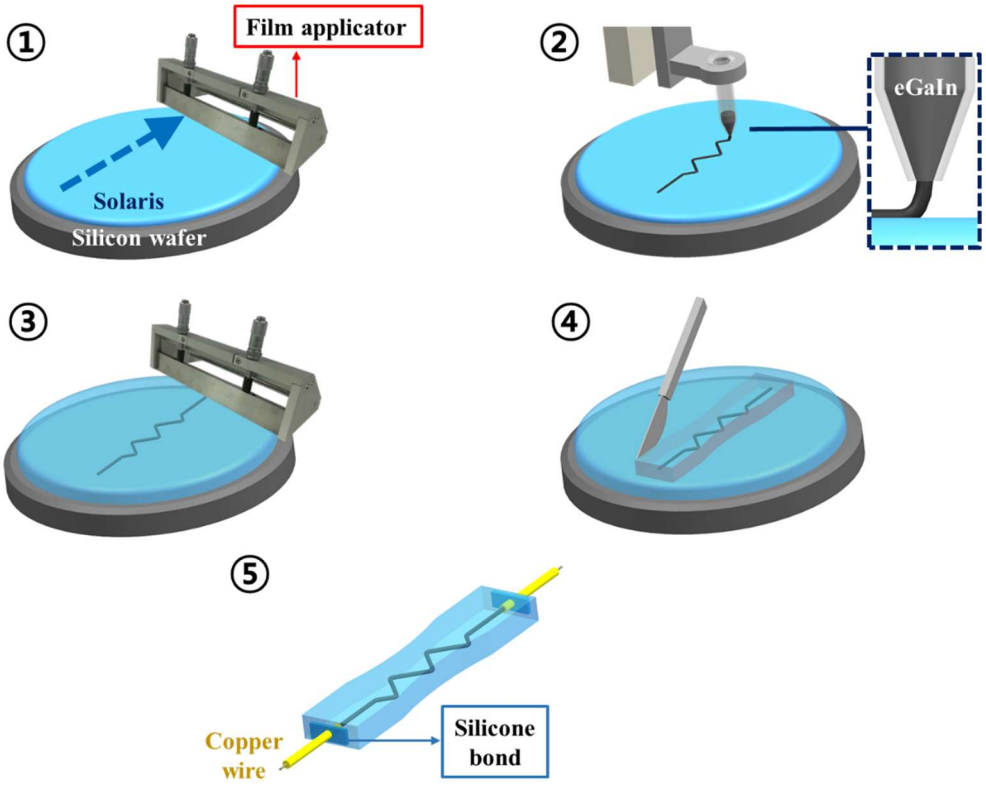

Figure 3.1 Fabrication of verification samples

3.1.2 The printable area on the elastomer layer

In particular, the direct ink writing enables the eGaIn wire to be drawn in various trajectories (Figure 3.2) with significant consistency in its cross-sectional area [18]. During the direct ink writing of eGaIn, a tendency of eGaIn to stick to the elastomer substrate due to the visco-elastic adhesion triggered by its oxide layer is used [44]. In other words, when an ejection tip [45] is located at a certain distance from the substrate, eGaIn itself comes out from the tip and tends to stick to the substrate. It implies that the sudden changes in the gap between the tip and the substance can keep eGaIn from ejection. To make it worse, Solaris has a low viscosity (about 1200 centipoises), which leads to non-flatness by flowing down from the silicon wafer. It reduces the printable area, where eGaIn wires can be drawn on Solaris, thus, the printable area must be examined. Figure 3.3 shows the flatness of Solaris layers estimated by visual measurements of changes in the gaps between the tip and Solaris with a microscope [46]. Based on empirical experiences, the eGaIn wire is not drawn if the change in the gap between the tip and the substrate is more than 0.03 mm, therefore, the printable area is set to a circle with a radius of 50 mm relative to the center of the silicon wafer, on the basis of the measured flatness. All eGaIn wires in this thesis are drawn on this printable area.

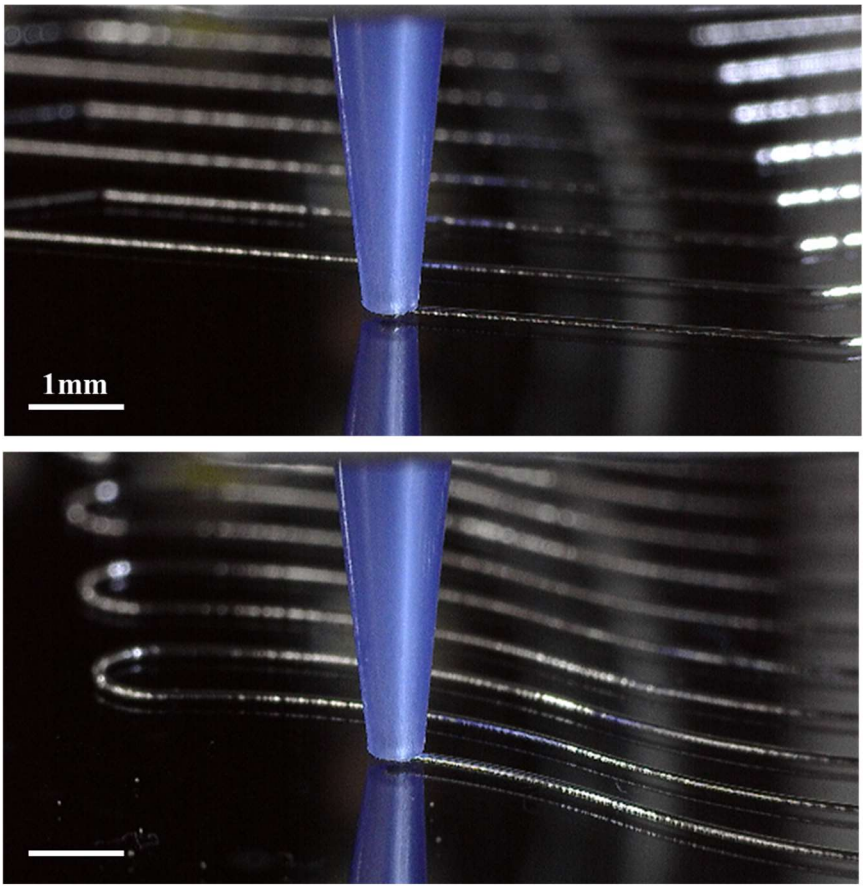

Figure 3.2 Direct ink writing of eGaIn to draw diagonal (top) and arc (bottom) patterns

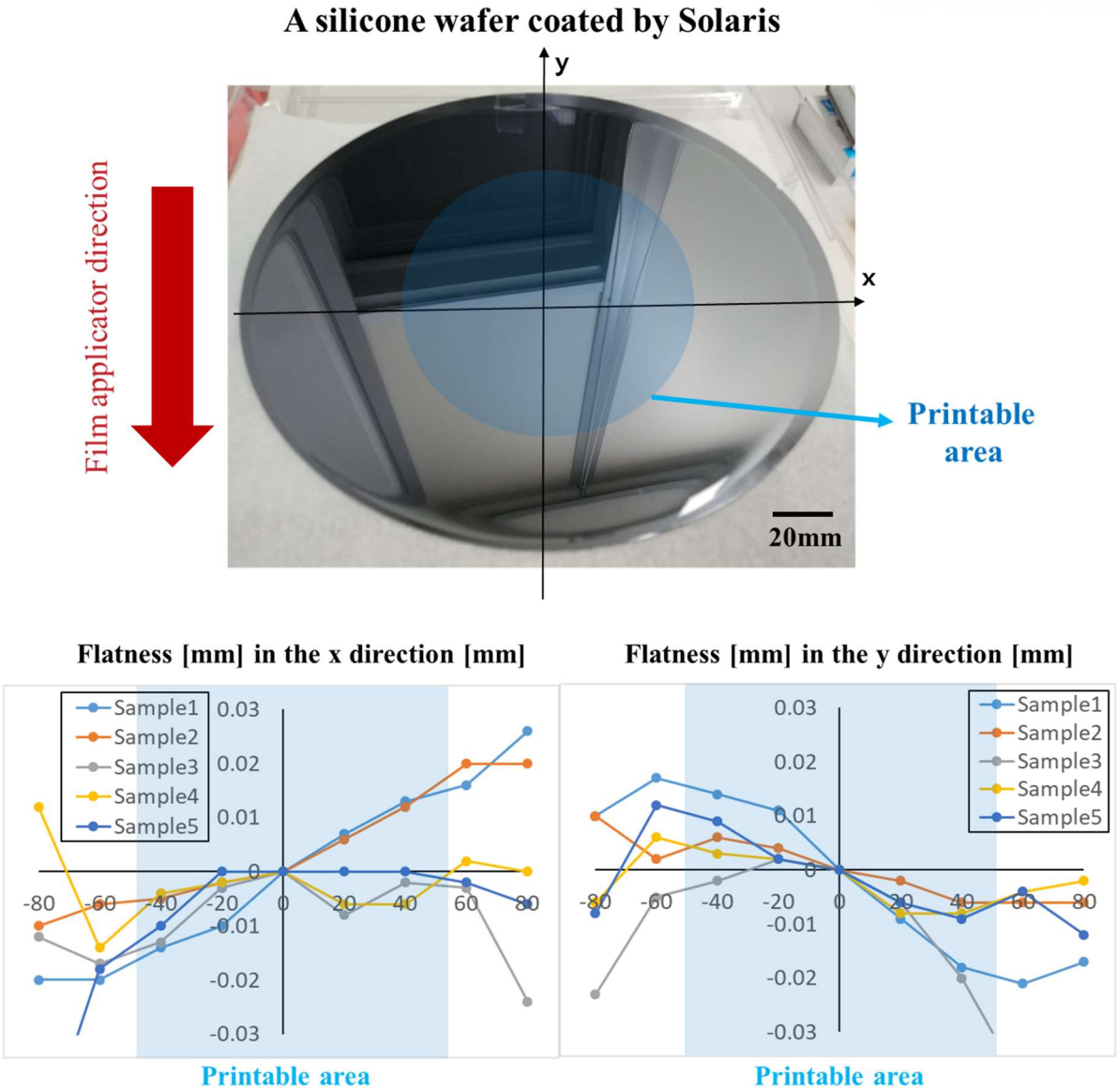

Figure 3.3 Measured changes in the flatness of Solaris samples

3.1.3 Determination of the contour of the verification samples

Another challenge during the fabrication was to determine the contour of samples. Although the fracture strain of Solaris written on its specification sheet is about 300% [37], some rectangular Solaris samples have been observed to be broken at a less than 120% strain, as shown in Figure 3.4, where the fracture of samples has occurred in the boundary between the static and stretchable parts.

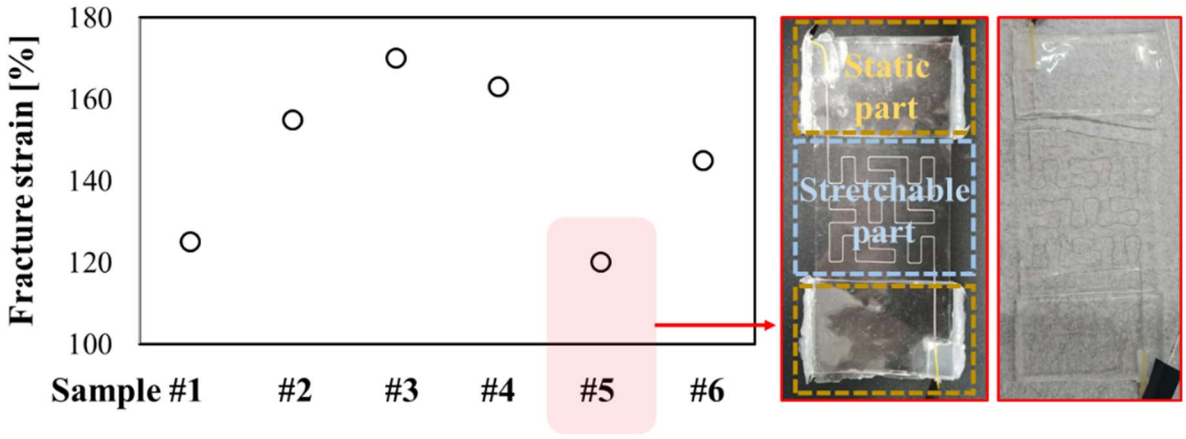

Figure 3.4 Fracture strain values of rectangular Solaris samples

It is supposed that the stress concentration, caused by the flowing of the internal stress through the narrow area, was the major reason for the fracture. If the area of the static part is widened, the stress concentration is expected to be reduced. With a computer-aided engineering (CAE) program [47], the stress distributions of rectangular and dumbbell-shaped samples under 100% strain have been examined. For the properties of elastomer required for the simulation, the study on polydimethylsiloxane (PDMS) was referred to [48]. As boundary conditions, one side of each sample was fixed and another side was pulled. The simulation results show that the maximum stress of the dumbbell-shaped sample was one-third that of the rectangular sample (Figure 3.5). Reflecting on these results, all samples in this thesis were fabricated in the dumbbell shape.

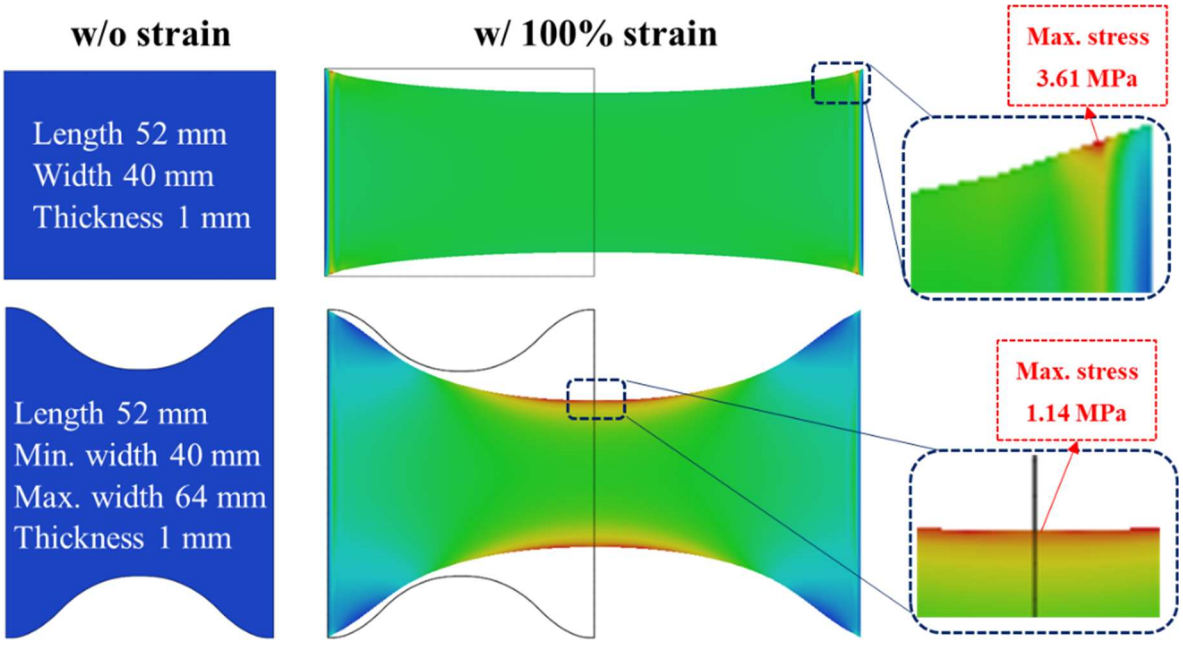

Figure 3.5 Simulation results of strained rectangular and dog bone-shaped samples

3.1.4 Signal input process during tensile tests

For testing the fabricated samples, the both ends of samples were fixed to a 3-axis robot [49], as shown in Figure 3.6. The samples were elongated up to 150% strain and returned to 0% strain with a strain rate of 5 mm/s depending on the operation of the robot. During the tensile tests, changes in the length of the samples were measured by a laser displacement sensor [50] and used to calculate the uniaxial strain applied to the samples. Resistance values of the samples were measured by employing a customized amplifier board and data acquisition (DAQ) [51]. The signals from the laser sensor and amplifier were input into a signal processing software [52] with a sampling rate of 100 Hz (Figure 3.7).

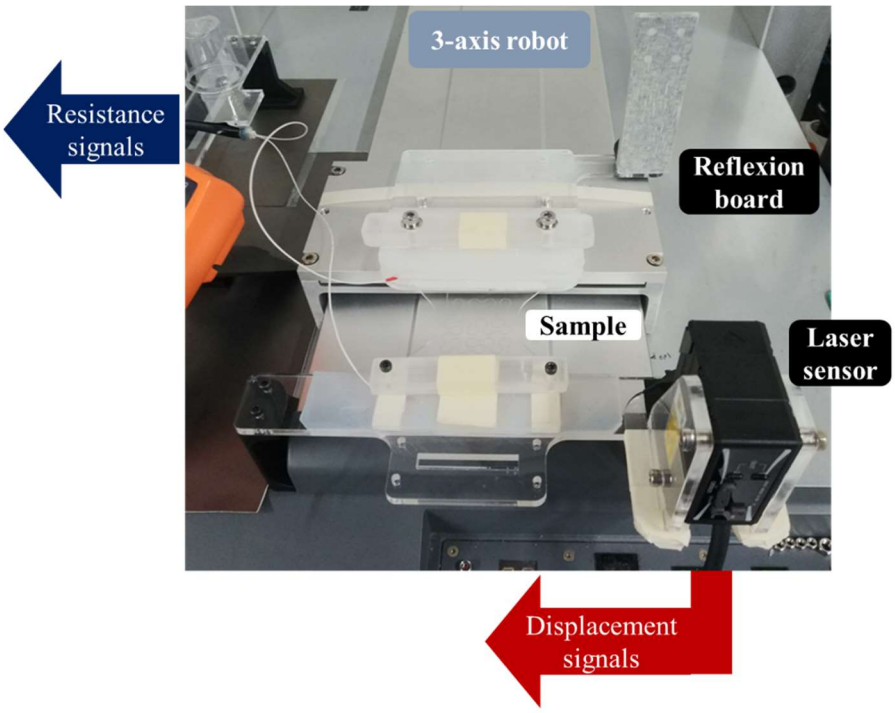

Figure 3.6 A sample fixed to a 3-axis robot

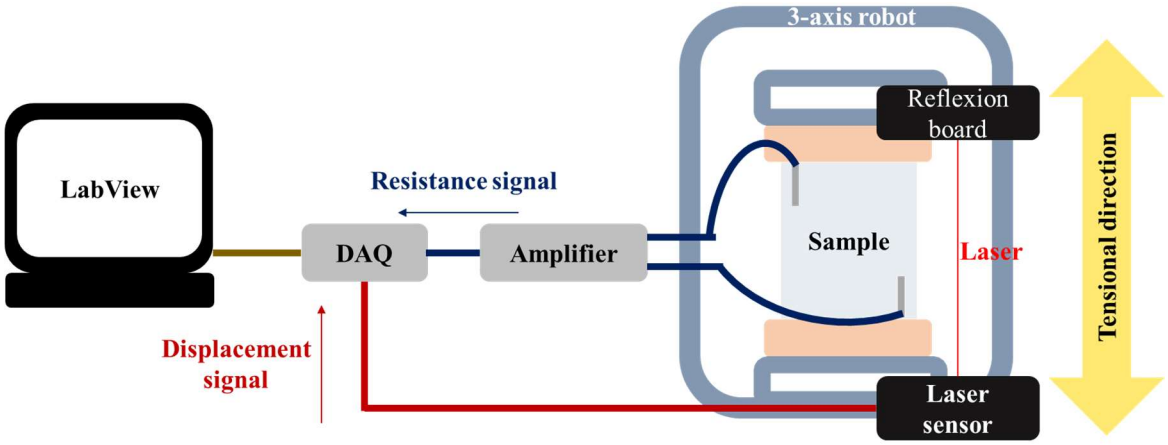

Figure 3.7 Signal input process

3.2 A method for applying the estimation models

3.2.1 An equation for applying estimation models

Before estimating the resistance changes in the verification samples under strain, the eGaIn wire in each sample was segmented into static, linked, and patterned parts as shown in Figure 3.8. Under strain, the static parts in the eGaIn wire were fixed to the tensile test robot, so, had unchangeable resistance values due to absence of elongation. On the contrary, the resistance values of the linked and patterned parts were changeable according to elongation. The linked part included tensional directional eGaIn wires, which connected between the static and patterned parts. The patterned part included an eGaIn wire patterned with diagonal lines or circular arcs. Reflecting these segmented three parts, the resistance changes in the verification samples under strain can be expressed with following equation (3.1), where the initial length ratio of the static, linked, and patterned parts to the total eGaIn wire are represented by α, β, and γ, respectively.

$$\left(\frac{R}{R_0}\right)_{\text{estimated}} = \alpha + \beta\left(\frac{R}{R_0}\right)_{\text{linked}} + \gamma\left(\frac{R}{R_0}\right)_{\text{patterned}} \tag{3.1}$$

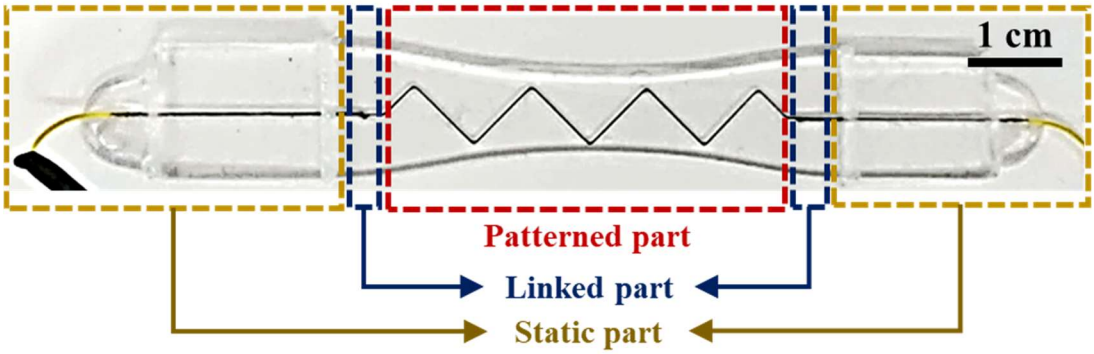

Figure 3.8 A sample segmented into static, linked, and patterned parts

On the right side of equation (3.1), the resistance change in the linked part in the second term is substituted by the resistance estimation model for a tensile directional eGaIn wire, equation (2.6). The resistance change in the patterned part in the third term is substituted by the resistance estimation model for a diagonal eGaIn wire or circular arc-shaped eGaIn wire, equation (2.11) or (2.16), in accordance with whether the pattern of the eGaIn wire is based on a diagonal line or a circular arc. Resistance changes in all verification samples are estimated with equation (3.1) hereafter.

3.2.2 An assumption for applying estimation models

The direct ink writing technique allows the consistent eGaIn wires to be drawn [18] and permits resistance values per unit length to be the same in the entire eGaIn wire. The length value of each eGaIn wire part can be given by the design dimensions of the eGaIn wires. Figure 3.9 shows the highly linear relationships between the total length and total resistance of eGaIn wires in the fabricated samples with a coefficient of determination of 98.78%, and it supports that the drawn eGaIn wires were consistent. Detailed data of Figure 3.9 are in Table 3.1. It seems that slight errors in the linear relationship have resulted from the inconsistent insertion of copper wires into eGaIn wires during fabrication, which makes the resistance values of the static parts inconsistent among the samples. Nevertheless, the inconsistent insertion of copper wires made no critical error, therefore, was ignored.

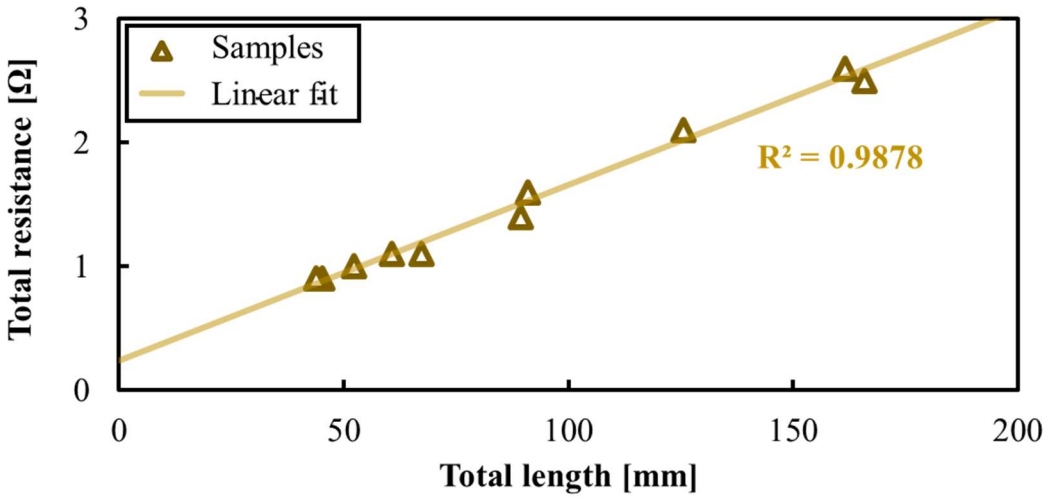

Figure 3.9 Relationship between total resistance and total length of eGaIn wires

Sample	Diagonal #1	Arc #1	Arc #2	Diagonal #2	Arc #3	Arc #4	Diagonal #3	Diagonal #4	Diagonal #5	Arc #5
Total Length [mm]	43.36	44.80	51.82	60.28	66.79	89.00	90.45	125.11	161.02	165.37
Total resistance [Ω]	0.9	0.9	1	1.1	1.1	1.4	1.6	2.1	2.6	2.5

Table 3.1 Data of total resistance and total length of eGaIn wires

3.3 Tensile test results

3.3.1 Patterns of verification samples

For the verification of the resistance estimation models for diagonal and circular arc-shaped eGaIn wires, samples were fabricated to have eGaIn wires patterned by diagonal lines of the verticalities between 0 and 4 and circular arcs of the starting angles and ending angles between 0° and 90° (Figures 3.10). The direct ink writing technique, which has flexibility in modification of eGaIn wire trajectories due to no need for any mold base or stencil, allowed a variety of patterns to be drawn quickly and economically [18], and has helped to fabricate the diagonal and arc-shaped patterned samples. The eGaIn wire trajectories were designed by using a computer-aided design (CAD) [53].

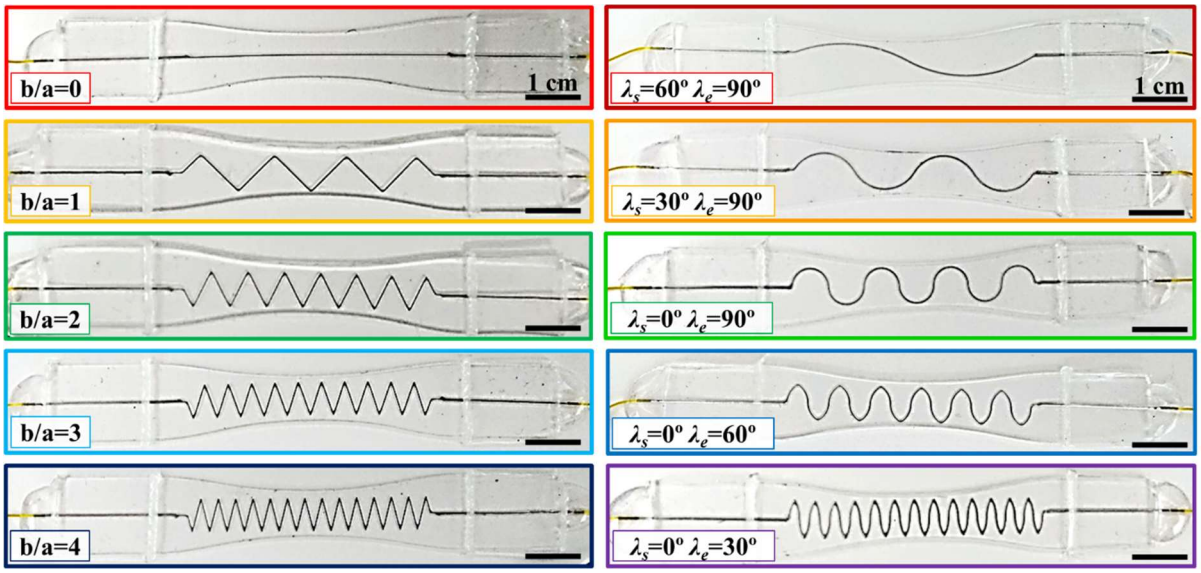

Figure 3.10 The fabricated samples with diagonal (left column) and arc (right column) patterns

3.3.2 Comparison between the measured and estimated resistance values

The resistance changes estimated by equation (3.1) were compared to the resistance changes measured during the tensile tests. Figure 3.11 shows the 150% strained samples during the tensile tests. The results of the tensile tests demonstrated that the estimated and measured resistance changes were extremely similar to each other in all samples and the dissimilarities between both resistance values were less than 0.05 in terms of a root mean square error (RMSE) as shown in Figures 3.12 and 3.13. It leads to the conclusion that the resistance estimation models can yield a highly precise estimation.

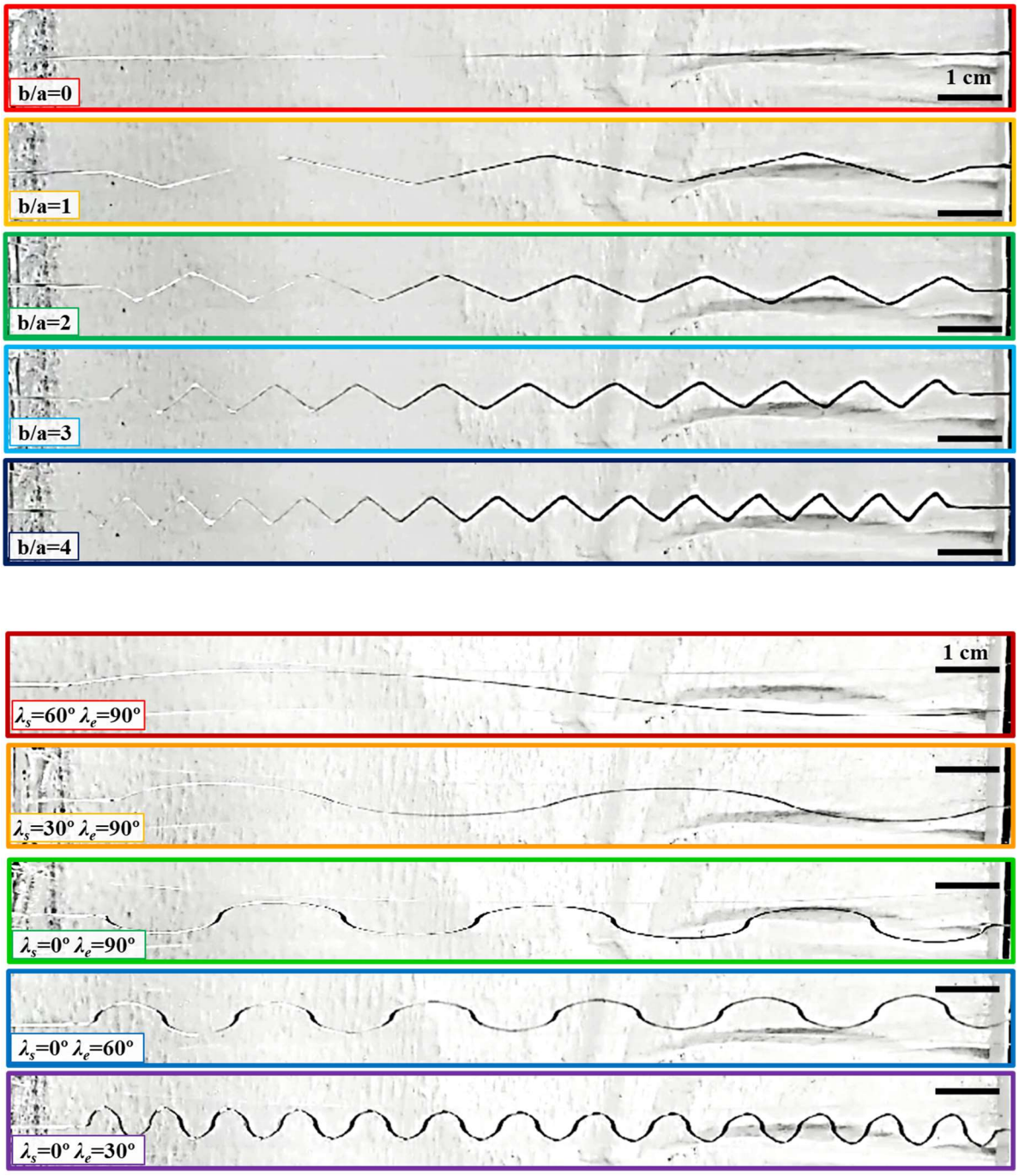

Figure 3.11 Samples under 150% strain

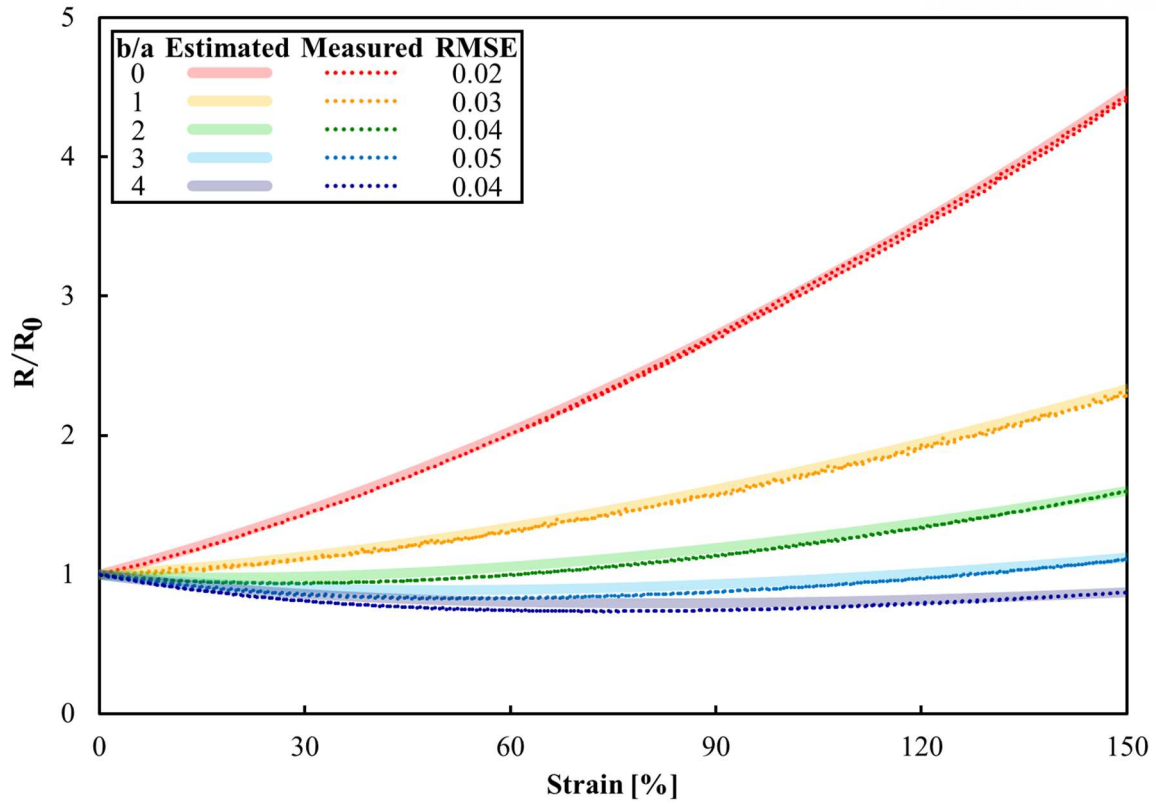

Figure 3.12 Measured and estimated resistance changes in samples patterned by diagonal lines

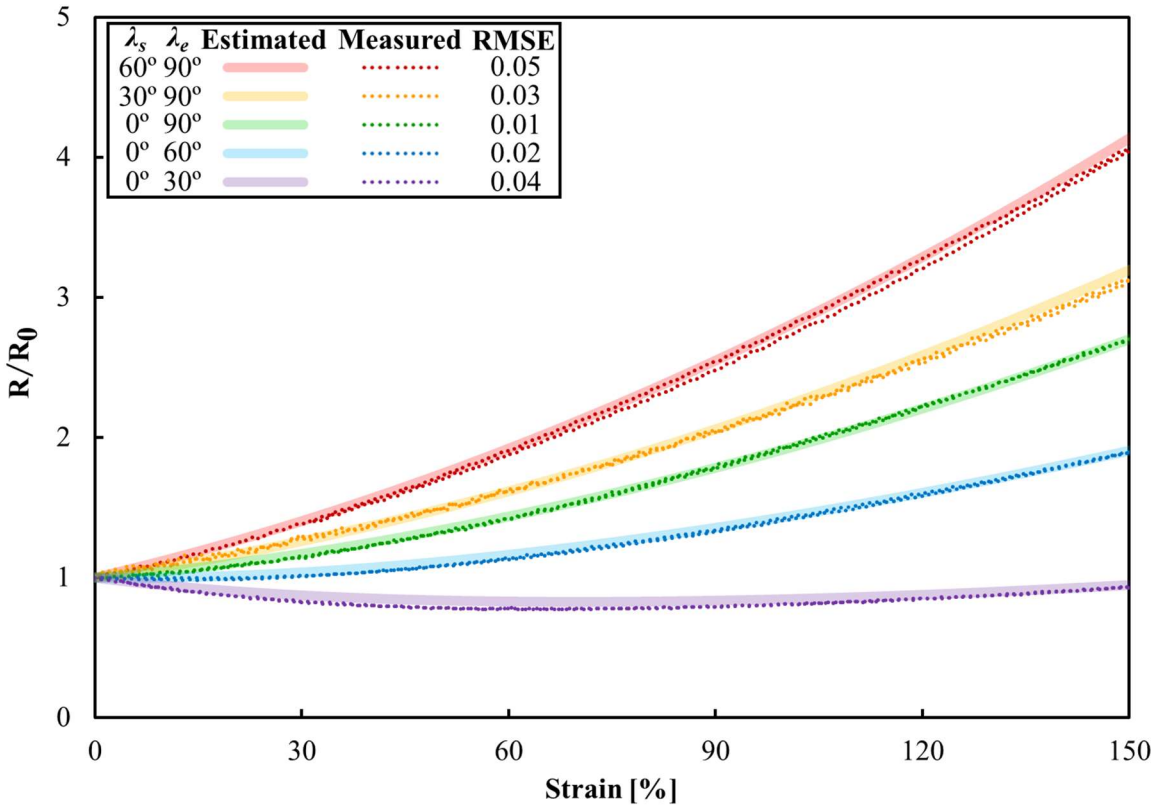

Figure 3.13 Measured and estimated resistance changes in samples patterned by circular arcs

However, the slight errors in the estimation were not avoidable due to the inconsistent insertion of copper wires. Because it was carried out manually, copper wires were highly likely to be inserted into eGaIn wires at inconsistent depths. As a result, it contributed to the denial of the underlying assumption that the lengths of the static parts of the eGaIn wires shown in Figure 3.8 are the same as their design dimensions, and each sample had a distortion in its value of variable α in equation (3.1). Besides, the randomness in the RMSEs of Figures 3.12 and 3.13 supports the opinion that the copper wire insertion was the main cause of the errors when considering that the copper wire insertion had no relationship with any parameters such as the length or pattern shape of eGaIn wires in the samples. Though, the errors from the copper wire insertion are expected to be reduced by increasing the proportion of the patterned eGaIn wire to the entire eGaIn wire so that the effects of the uncertainty in the copper wire insertion are decreased.

3.3.3 Minor reasons for estimation errors

It seems that another assumption that the elastomer is iso-volumetric also had a minor issue. It has been proved that elastomer silicones cannot be completely iso-volumetric theoretically and experimentally [18, 32, 54, 55]. If a material is iso-volumetric, its Poisson's ratio (v) is 0.5, but for most materials including Solaris, their Poisson's ratios are less than 0.5, which means that under uniaxial strain, the actual transverse deformation of them is smaller than the ideally iso-volumetric one. Generally, volumes of actual materials increase under strain, as equation (3.2) and Figure 3.16 implies.

$$\frac{V}{V_0} = (1+\varepsilon)(1-v\varepsilon)^2 \begin{cases} = 1 & (\text{when } v = 0.5) \\ > 1 & (\text{when } v < 0.5) \end{cases} \tag{3.2}$$

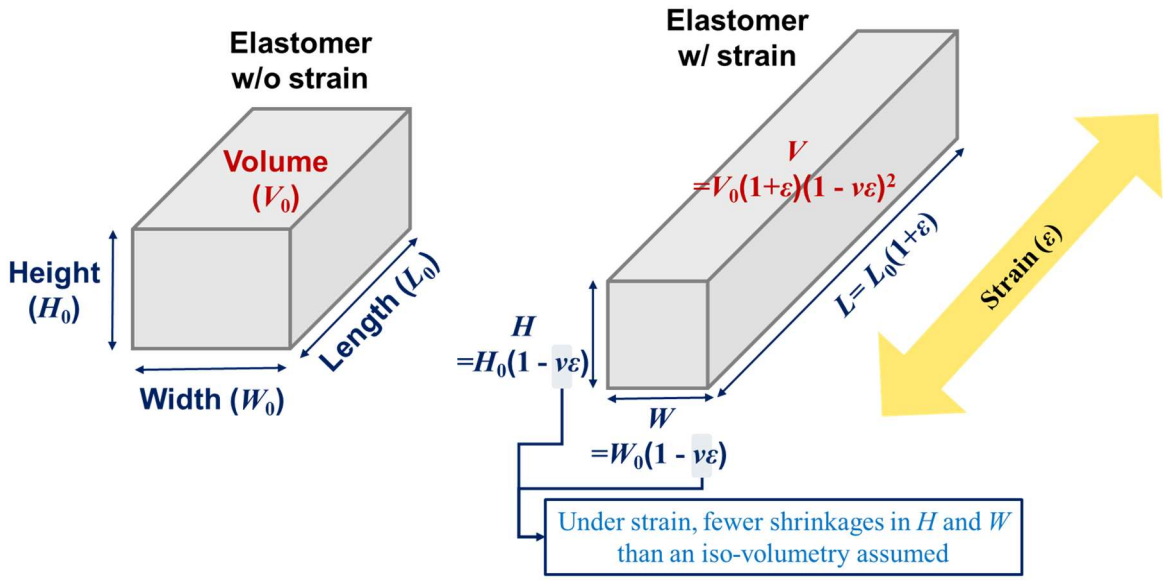

Figure 3.14 Volume changes in elastomer under strain

The increased volume of the strained Solaris was observed with a brief test. When a Solaris sample embedding eGaIn was under strain, eGaIn was sucked in a little (Figure 3.15). It was due to the increased volume in the micro-channel occupied by eGaIn wire while eGaIn had no volume change. Still, the impact on volume changes in Solaris appeared to be much small in that less than a drop of eGaIn was dragged in when the eGaIn wire of total length of 1000 mm was under 50% strain. Thus, the error triggered by the increased volume was treated as negligible.

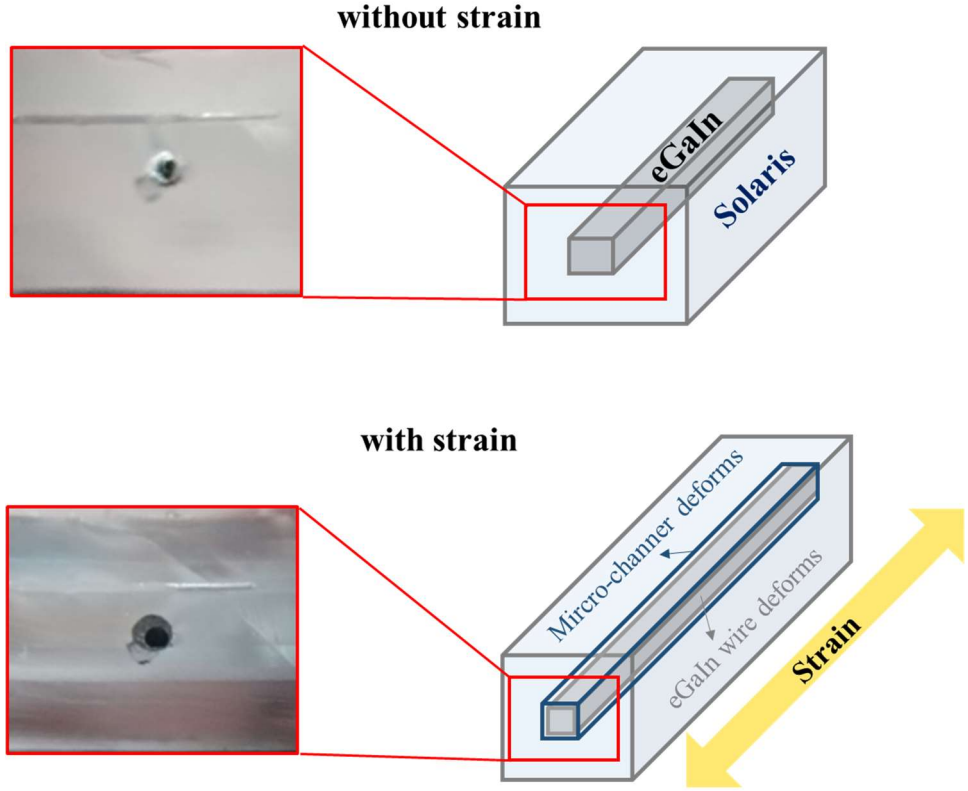

Figure 3.15 Cross-sections of Solaris embedding eGaIn with and without strain

Hysteresis, which is defined as the difference between resistance values under strain and return, was another issue related to the estimation error. Hysteresis can be calculated by the following equation (3.3), and was less than 5.9% in all samples during 150% strain (Table 3.2). The maximum hysteresis occurred in the sample patterned by an arc with a starting angle of 30° and an ending angle of 90°, and electrical noises engaged in this sample seemed to be the primary cause for the hysteresis as shown in Figure 3.16. However, the estimation errors are still small regardless of the hysteresis, and the strain rate, the main reason for hysteresis, is not contained in estimation models. Accordingly, hysteresis was not analyzed in this thesis, and reference to a study on hysteresis is recommended for more information on hysteresis in stretchable sensor [56].

$$\text{Hysteresis} = \frac{R_{\text{strain}} - R_{\text{return}}}{R_{\text{strain}}} \tag{3.3}$$

Sample	Diagonal #1	Diagonal #2	Diagonal #3	Diagonal #4	Diagonal #5	Arc #1	Arc #2	Arc #3	Arc #4	Arc #5
Maximum hyteresis	1.61%	2.91%	1.07%	1.55%	1.06%	3.00%	5.88% (Max)	1.71%	2.01%	1.68%

Table 3.2 Maximum values of hysteresis in all verification samples

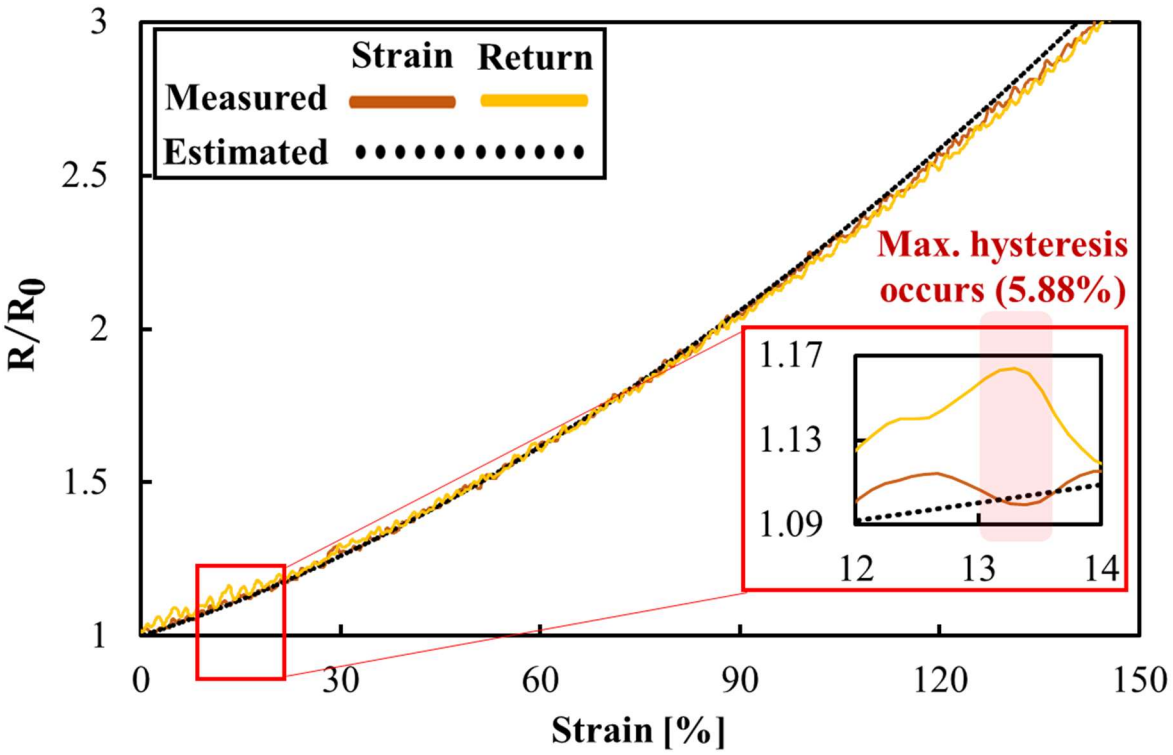

Figure 3.16 The maximum hysteresis of the arc sample #2

In Chapter 3, the derived estimation models have been verified to offer a precise estimation of resistance changes in the diagonal and circular arc-shaped eGaIn wires in a strain range of 0~150%. In the next Chapter, these estimation models are applied to an eGaIn-based strain sensor and heater.

Chapter 4. Applications

4.1 Estimation on resistance changes in an eGaIn-based strain sensor

4.1.1 Limits for existing analysis on resistance changes

Although eGaIn strain sensors in previous studies have semicircular eGaIn wires, resistance changes in the eGaIn sensors under strain have been estimated with the assumption that the semicircular eGaIn wires are short enough to be negligible [18, 24]. It was obvious that estimation errors were followed because the deformation of the semicircular eGaIn wires under strain affected the resistance changes in the eGaIn sensors.

To verify the effects of semicircular eGaIn wires on resistance changes in an eGaIn sensor, a tensile test was conducted. An eGaIn sensor having semicircular wires was fabricated and tested in the same method as the aforementioned for the verification samples. Figure 4.1 presents the fabricated sensor, whose eGaIn wire is segmented into stationary, longitudinal, and semicircular parts. Resistance changes in the eGaIn sensor were estimated by corresponding the stationary, longitudinal, and semicircular parts to the first, second, and third terms on the right side of equation (3.1). The semicircular eGaIn wires were regarded as circular arcs with a starting angle of 0° and an ending angle of 90°.

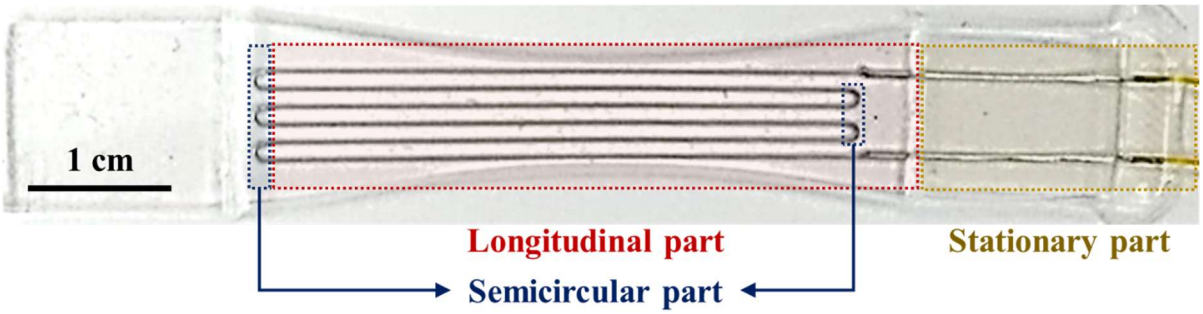

Figure 4.1 The fabricated eGaIn strain sensor

4.1.2 Tensile test results

Figure 4.2 presents the result of the tensile test with the eGaIn sensor in a strain range of 0~150%, showing the resistance changes measured and estimated with and without considering the semicircular parts. Though the total length of all the semicircular parts takes up only 3% of the entire length of the wire in the eGaIn sensor, the resistance values estimated considering the semicircular parts were closer to the measured resistance values with a 56.07% reduction in estimation error, compared to the resistance values estimated without the semicircular parts.

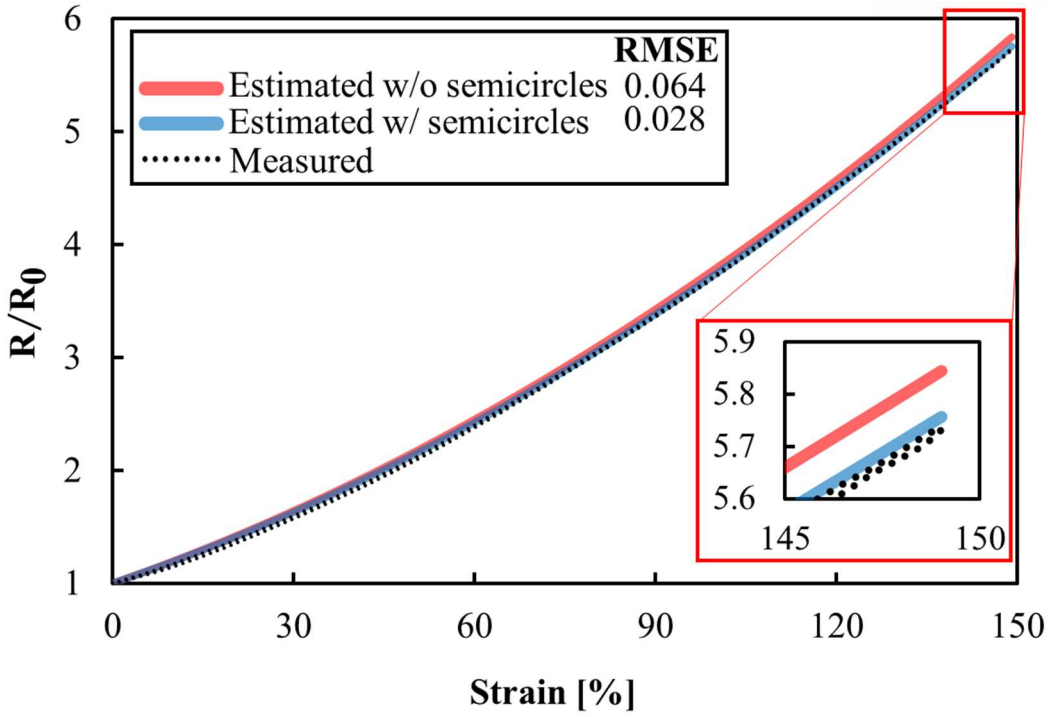

Figure 4.2 The measured and estimated resistance changes in the eGaIn sensor under strain

In other words, the tensile test result lends support to the assertion that the estimation error is significantly reduced when the resistance change under strain is estimated considering the semicircular eGaIn wires. In practice, the exclusion of the semicircular wires in estimating the resistance changes in the eGaIn sensor containing the semicircular wires means that the entire deformable wire in the eGaIn sensor is regarded as the linear wire. However, the difference in the resistance change in the linear and semicircular eGaIn wires under strain clearly exists as shown in Table 4.1: the resistance values of the linear eGaIn wire are 1.25 times, 1.51 times, and 1.64 times those of the semicircular eGaIn wires at 30%, 90%, and 150% strain, respectively. It can be concluded that these differences, which grow up when more strain is applied, increase the estimation error when estimating the resistance change without considering the semicircular eGaIn wires. Thus, the estimation model for the circular arc-shaped eGaIn wires is expected to help in the precise estimation of resistance changes in eGaIn-based electronics, containing semicircular wires and targeting ultra-stretchability, under strain.

Strain		30%	60%	90%	120%	150%
Resistance changes under strain	**Semicircular eGaIn wire ($(R/R_0)_S$)**	1.4299	2.0112	2.7167	3.5254	4.4393
	Linear eGaIn wire ($(R/R_0)_L$)	1.1444	1.4259	1.7957	2.2224	2.7002
Difference ($(R/R_0)_S/(R/R_0)_L$)		1.2495	1.4105	1.5129	1.5863	1.6441

Table 4.1 Differences in resistance changes in the linear and semicircular eGaIn wires under strain

4.2 eGaIn patterning for a stretchable heater

4.2.1 Heating of stretchable heaters

The estimation models are applicable to the design of eGaIn heaters whose heating temperature is needed to be constant under strain. For this purpose, the resistance change for a constant temperature under strain must be revealed first. The heating of an eGaIn heater can be considered as a one-dimensional heat transfer with heat generation in a plate on the basis of the assumption that the patterned eGaIn wires act as a heating plate with a height small enough (0.1mm) to be ignored compared to that of the elastomer matrix (0.8mm) and are located in the center of the cross-section of the eGaIn heater as shown in Figure 4.3. In addition, the heating temperature, represented by T, is assumed to be only influenced by the thermal conduction of the elastomer matrix and convection with the air surrounding the eGaIn heater in the steady-state. Then, as shown in Figure 4.4, a temperature distribution in the cross-section of the eGaIn heater along the height direction, z-axis, can be expressed with an internal heat generation rate per volume, q_{gen}, and the height of the eGaIn heater, H, as following equation (4.1) where k is the conductivity of Solaris, T_a is the unchangeable temperature of the air, and h is the convection heat transfer coefficient of the air:

$$T(z) = T_a + \frac{q_{gen}H}{2h} + \frac{q_{gen}}{k}\left(\frac{H^2}{4} - z^2\right) \tag{4.1}$$

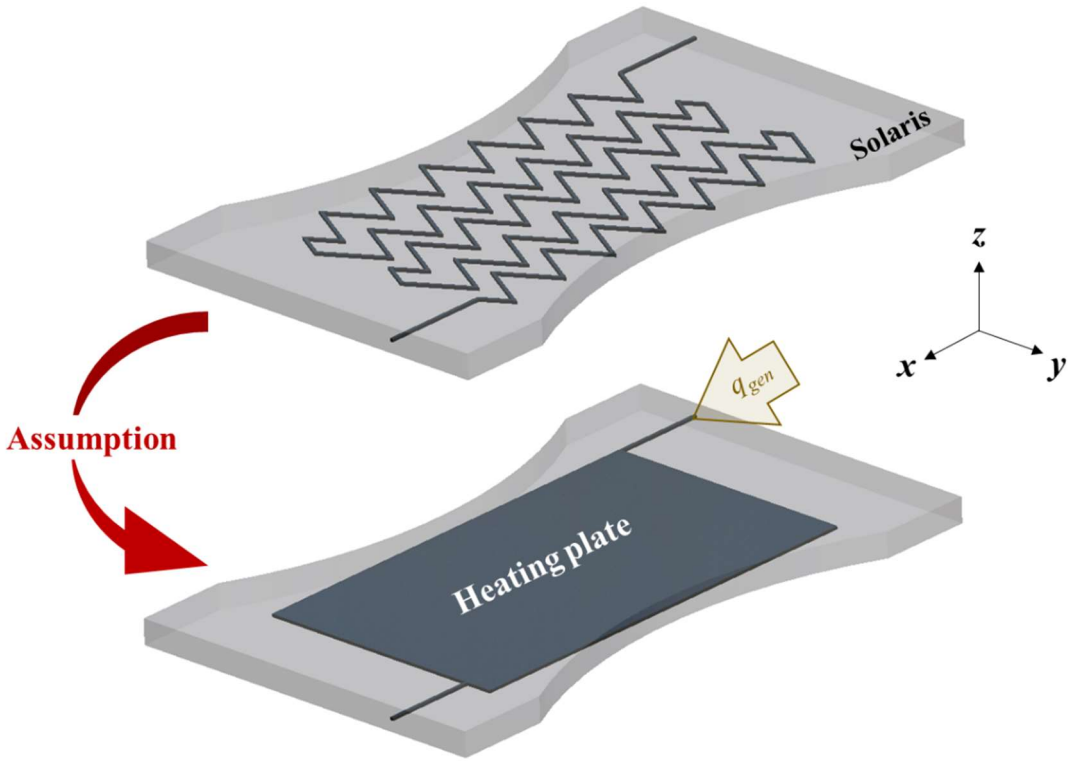

Figure 4.3 An eGaIn heater with and without the assumption

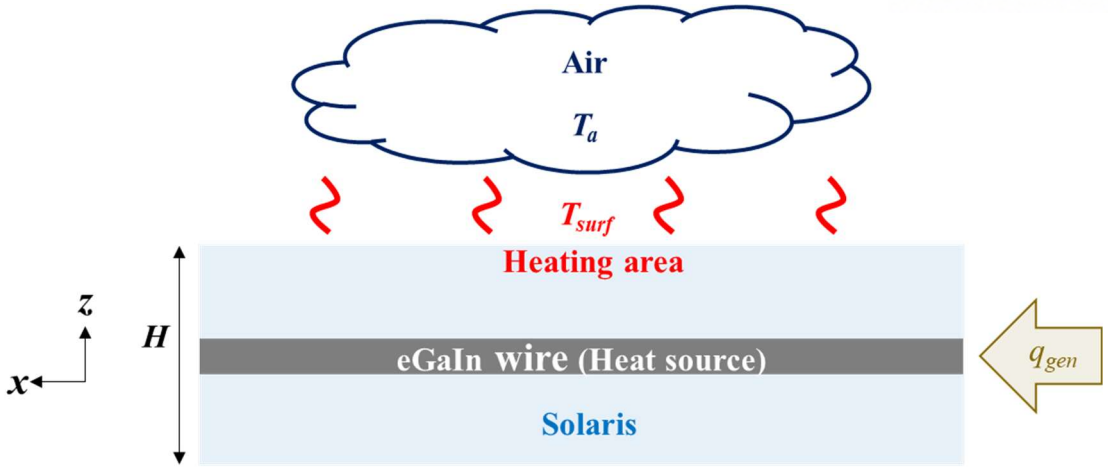

Figure 4.4 A cross-section of an eGaIn heater during heating

Here, the temperature of the surface of the eGaIn heater, T_{surf}, is given as follows:

$$T\left(\frac{H}{2}\right) = T_{surf} = T_a + \frac{q_{gen}H}{2h} \tag{4.2}$$

The difference in the temperature of the surface and air, $\Delta T = T_{surf} - T_a$, can be expressed as follows:

$$q_{gen} = \frac{2h}{H}\Delta T \tag{4.3}$$

If the temperature of the eGaIn heater has no change under strain, the variables relevant to temperature in equation (4.3), i.e., the convection heat transfer coefficient and the temperature difference, becomes constant. Then, the only one changeable variable on the right side of equation (4.3) is the height of the eGaIn heater. To put it another way, when the height is changed depending on the changes in the heat generation rate per volume, the heater can heat up with a constant temperature under strain. With the iso-volumetry, the heat generation rate per volume changes under strain as follows:

$$\frac{q_{gen}}{q_{gen,\,0}} = \frac{H_0}{H} = \frac{H_0}{H_0(1-\nu\varepsilon)} = \frac{1}{1-\nu\varepsilon} = \sqrt{1+\varepsilon} \tag{4.4}$$

The heat generation rate per volume means the heating power density per time and can be expressed with the voltage applied to the eGaIn heater, V_{app}, as follows:

$$q_{gen} = \frac{\frac{V_{app}{}^2}{R}}{Volume \times time} \tag{4.5}$$

The iso-volumetry makes the volume of Solaris constant, and the voltage per unit time, $V_{app}/time$, is uniform in virtue of the steady provision from a DC power supply [57]. Hence, the change in the heat generation rate per volume under strain can be represented by the reciprocal of the resistance change as follows:

$$\frac{q_{gen}}{q_{gen,\,0}} = \frac{R_0}{R} \tag{4.6}$$

By substituting equation (4.6) into equation (4.4), the resistance change required for the eGaIn heater under strain to heat up with a constant temperature is derived as follows:

$$\frac{R}{R_0} = \frac{1}{\sqrt{1+\varepsilon}} \tag{4.7}$$

Therefore, the wire of the eGaIn heater must be designed to have a resistance change similar to that presented by equation (4.7). Between the diagonal line and circular arc, the diagonal line was adopted for the pattern of the eGaIn heater because the deformation of diagonal patterns is equal in the whole wire unlike circular arc patterns whose deformation is partially different (Figure 4.5). In that the deformation contributes to the changes in the resistance and heating temperature as shown in Figure 4.6, arc patterns are likely to have uneven heating.

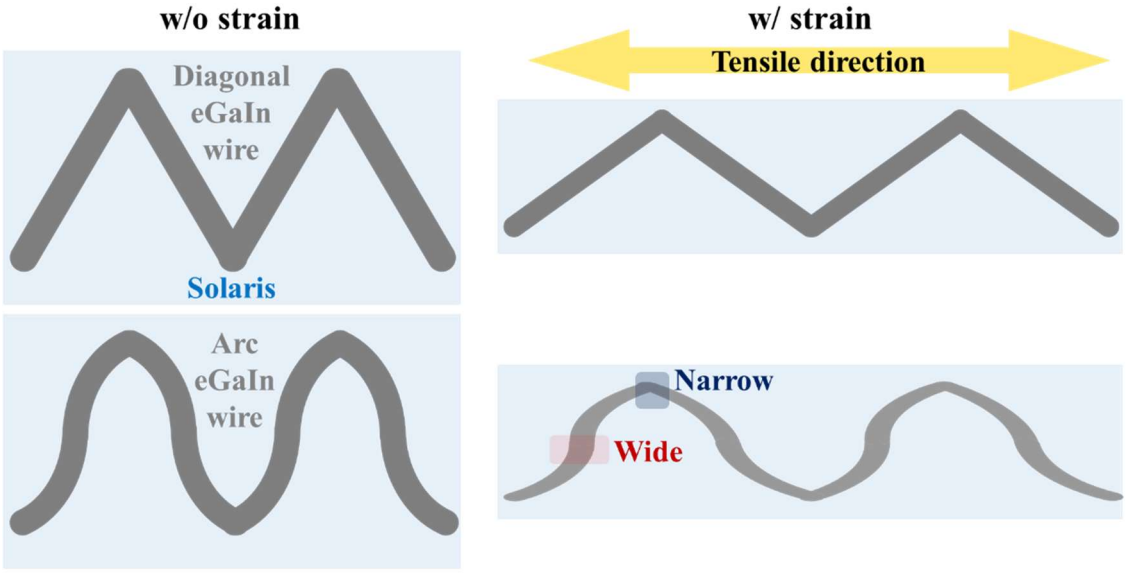

Figure 4.5 The deformation of the diagonal and arc patterns under strain

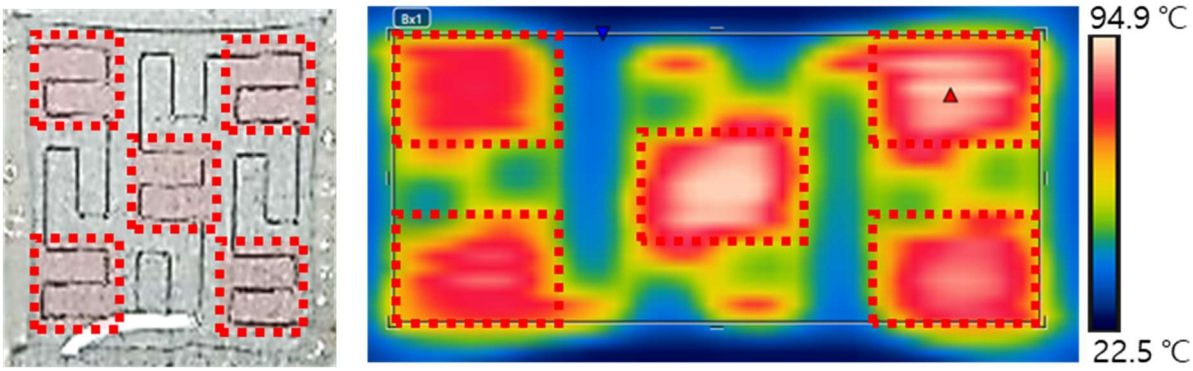

Figure 4.6 Heating temperatures in the tensile and tensile-vertical eGaIn wire parts under strain

4.2.2 Fabrication of stretchable heaters for verification

Now, the verticality of the diagonal line is determined. Figure 4.7 presents the estimated resistance changes in diagonal eGaIn wires with different verticalities (equation (2.11)) and the resistance changes for the constant temperature (equation (4.7)) in a strain range of 0~100%. Let us define “the extrema gap” as the gap between the maximum and minimum values of the difference between equations (2.11) and (4.7); as shown in Figures 4.8, 4.9 and Table 4.2, the extrema gap becomes the smallest when a verticality is 4. Therefore, an eGaIn wire patterned by the diagonal line with a verticality of 4 is used for the eGaIn heater.

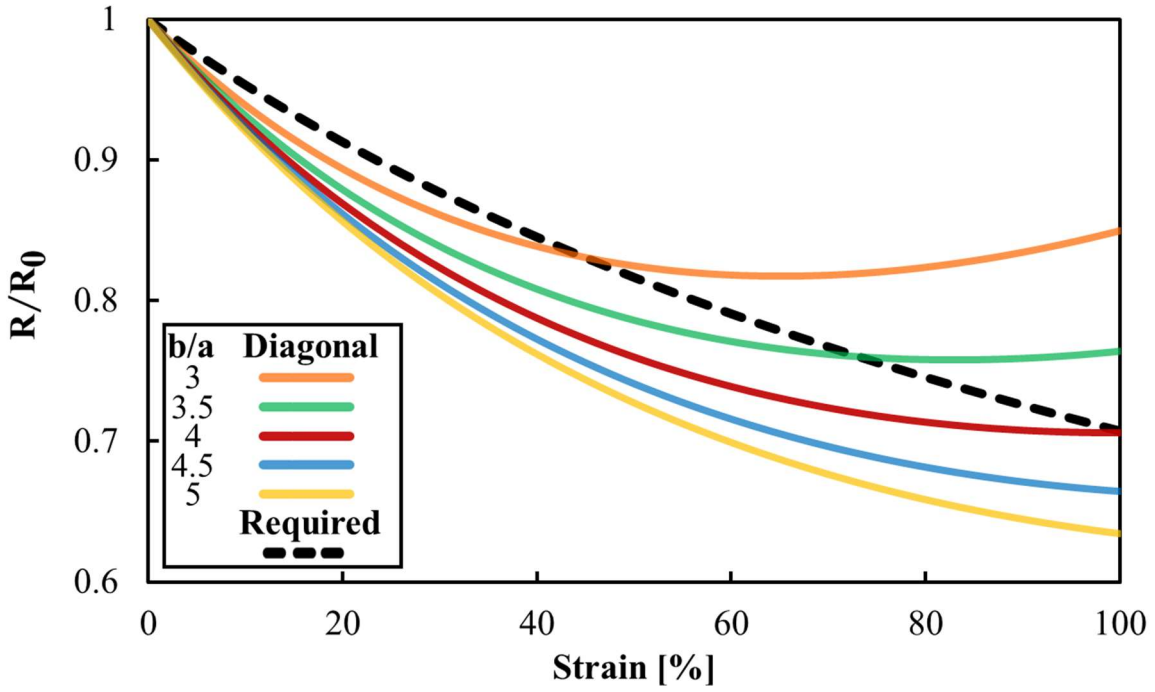

Figure 4.7 The estimated resistance changes in diagonal eGaIn wires and required resistance change for a constant temperature (black dotted line)

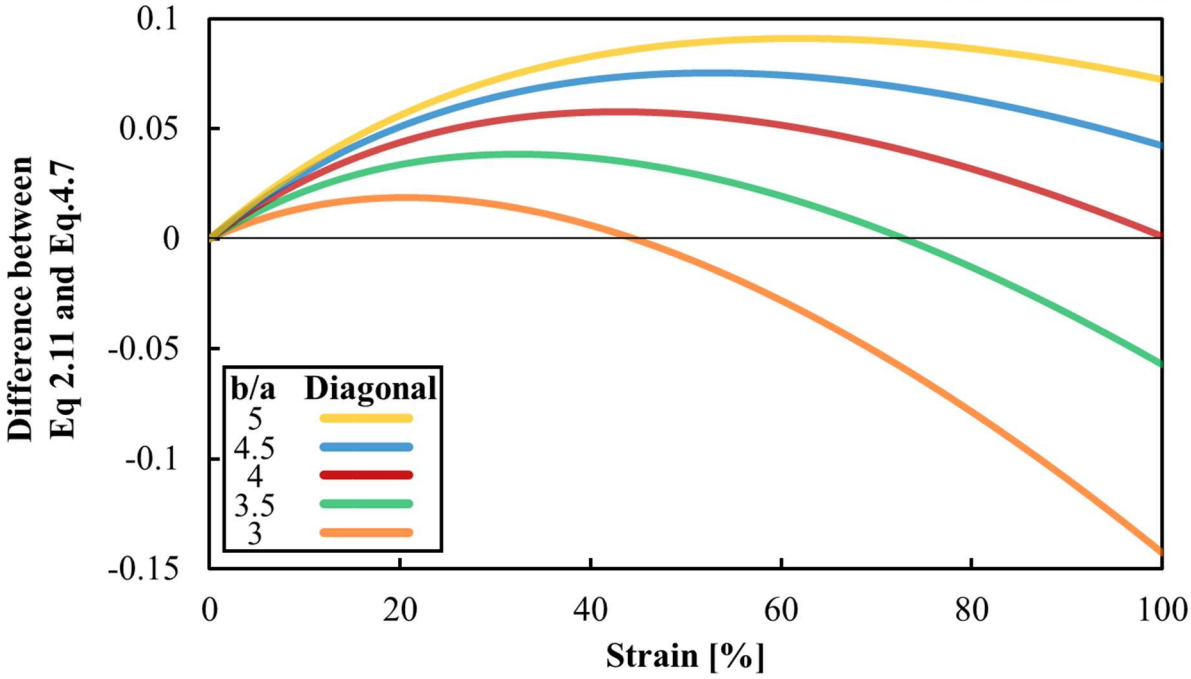

Figure 4.8 Differences between equations (2.11) and (4.7)

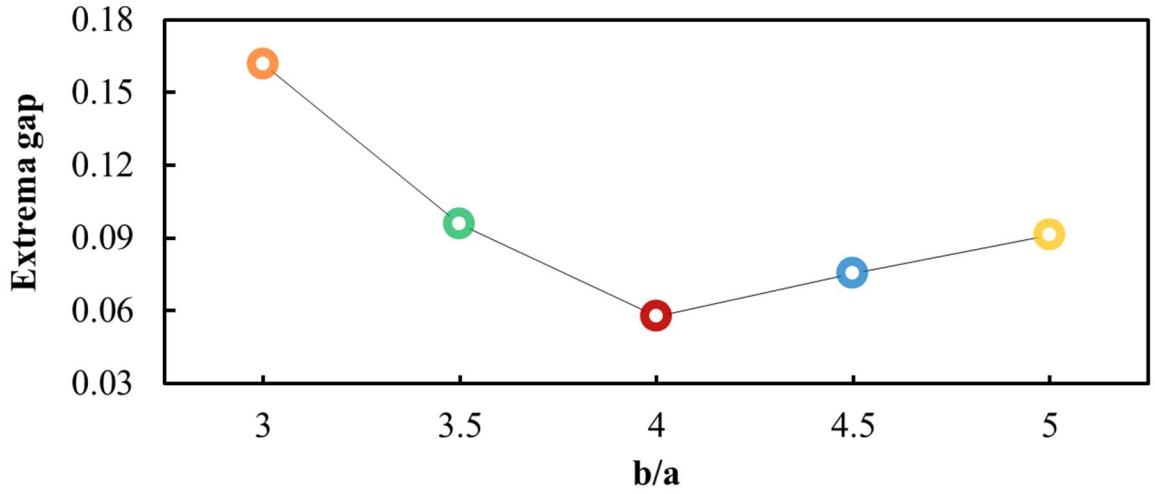

Figure 4.9 Extrema gaps according to the verticalities

Verticality (b/a)	3.5	3.6	3.7	3.8	3.9	4	4.1	4.2	4.3	4.4	4.5
Max. value of eq (2.11) – eq (4.7)	0.039	0.042	0.046	0.050	0.054	0.058	0.061	0.065	0.069	0.072	0.075
Min. value of eq (2.11) – eq (4.7)	-0.057	-0.044	-0.031	-0.020	-0.009	0	0	0	0	0	0
Extrema gap	9.6%	8.6%	7.8%	7.0%	6.3%	5.8% (min.)	6.1%	6.5%	6.9%	7.2%	7.5%

Table 4.2 Data of extrema gaps according to the verticalities

For verification, a diagonal heater and a comparison heater were respectively fabricated by patterning the diagonal eGaIn wire and the rectangular eGaIn wire, which consists of most tensile directional wires and slight tensile-vertical wires (Figure 4.10). The diagonal wire in the eGaIn heater occupies 99.8% of the length in the entire eGaIn wire to dominate the resistance change in the eGaIn heater under strain. The two fabricated heaters were tested in the same way as mentioned in Chapter 3, except that heaters were elongated up to 100%. Figure 4.11 presents the results of the tensile tests; in both samples, the estimated and measured resistance changes were greatly similar to each other with estimation errors of less than 0.026. Namely, resistance changes of the two heaters were realized as expected.

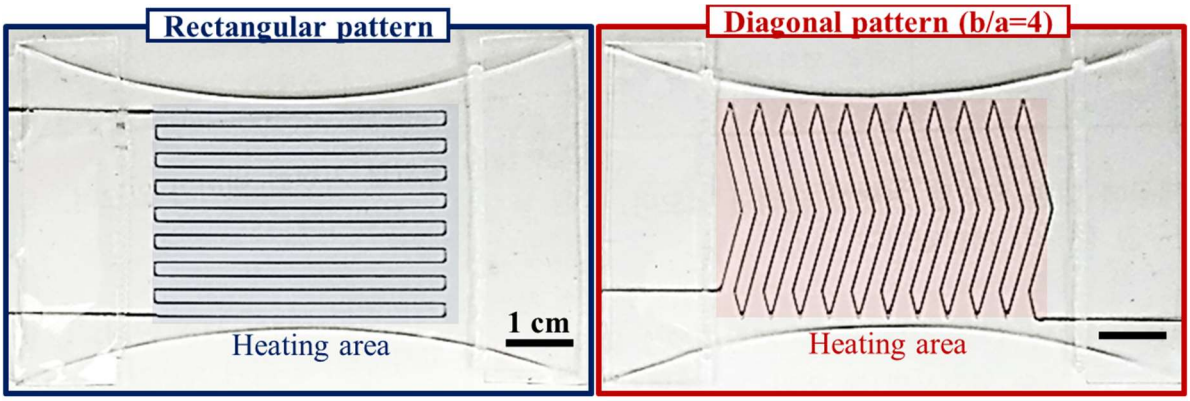

Figure 4.10 The fabricated heaters with the rectangular and diagonal patterns

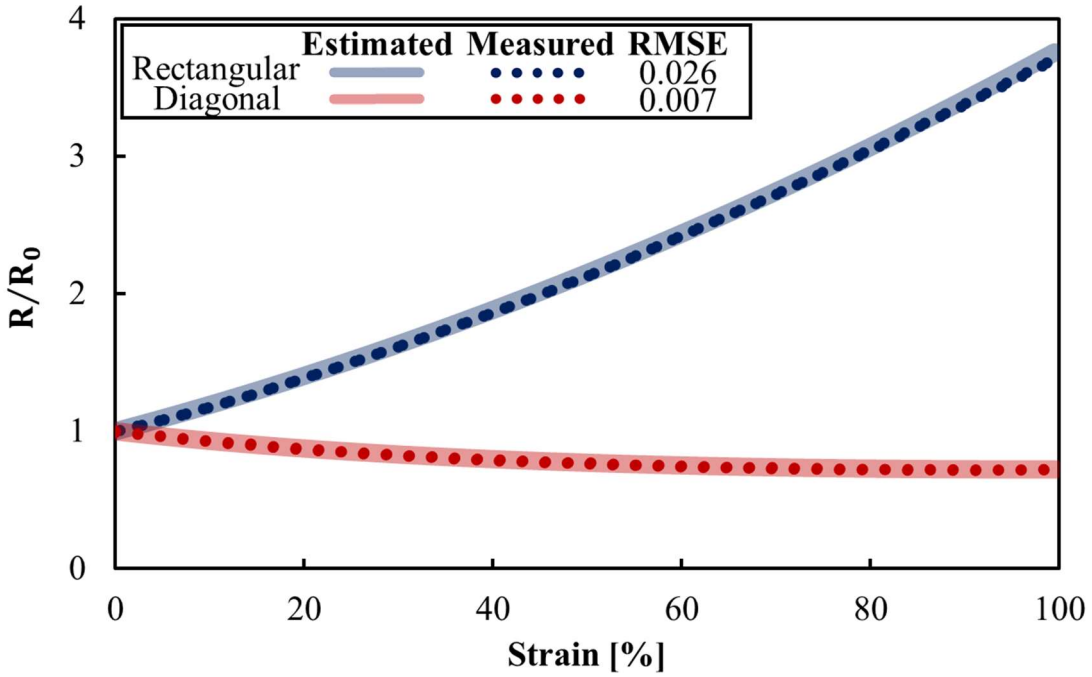

Figure 4.11 The estimated and measured resistance changes in the two heaters

In the tensile test results, it is notable that the estimation error of the diagonal patterned eGaIn heater was extremely small. Given that the total wire length in the diagonal patterned eGaIn heater was long (about 720 mm), it is natural that the estimation error of it can be small. The estimation error of the rectangular patterned eGaIn heater, whose total wire length is 700 mm, was also on the small side in comparison to the verification samples in Chapter 3. It seems that increased length in the total wire had been effective in the reduction in the randomness of the copper wire insertion.

4.2.3 Tensile-heating test results

Tensile-heating tests were conducted for examination of the temperature changes in the two heaters under strain by using an infrared camera [58], which has 1.5 mm^2 of a unit pixel accuracy. Figure 4.12 demonstrates the setup for tensile-heating test. As shown in Figure 4.10, the heater surfaces around the patterned wires were named “heating area” and mean values of heating temperature were calculated by dividing the summation of the measured temperature values of all pixels in the heating area by the number of the counted pixels. During the tensile-heating tests, a constant voltage, which generated an initial mean temperature of about 90°C, was engaged in each heater, and simultaneously the strain applied to each heater was increased step-wisely by 10% every 180 seconds until reaching 100%. The values of saturated temperatures were measured 170 seconds after each step-wise increase in strain and utilized to calculate the mean temperatures. Figure 4.13 presents the heating areas of the two heaters during the tensile-heating tests.

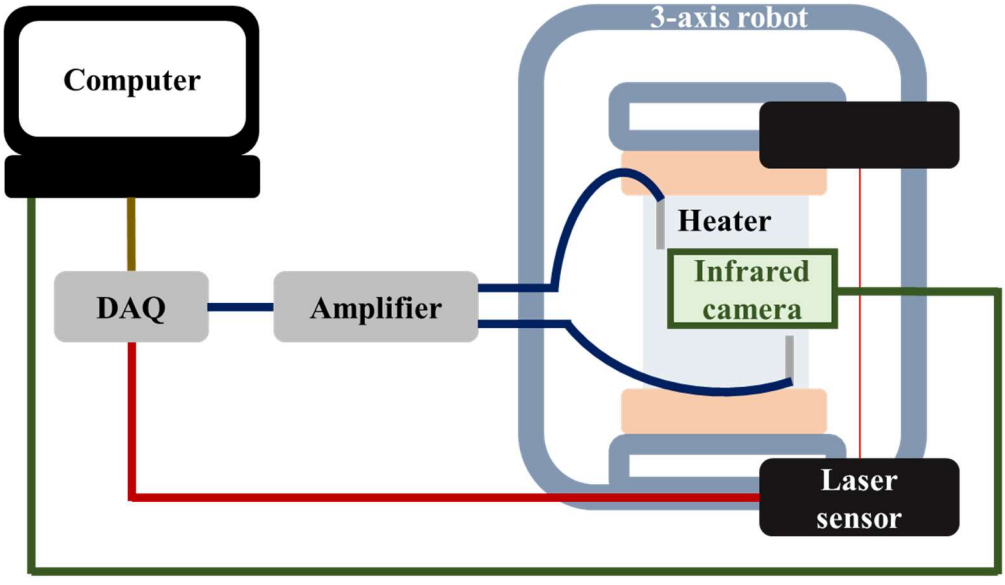

Figure 4.12 The setup for tensile-heating tests

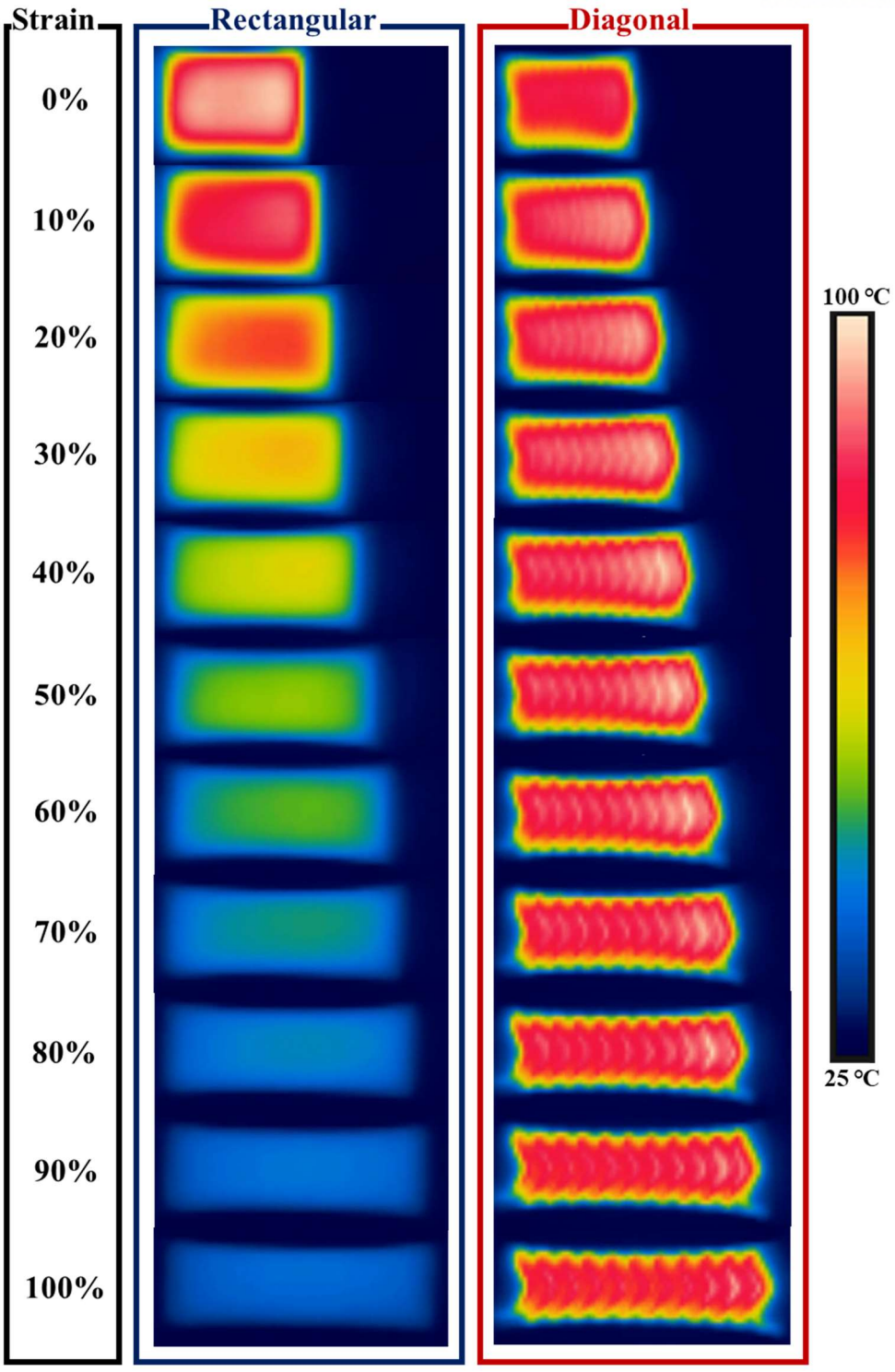

Figure 4.13 Heating areas of the rectangular and diagonal heaters during tensile-heating tests

Figure 4.14 presents the maximum temperature values in the heating area of two heaters, which were measured by the infrared camera at a speed of 3 Hz. It is confirmed that temperatures were saturated sufficiently 170 seconds after each increase in strain. The saturated maximum and mean temperatures of the two heaters depending on strain are presented in Figure 4.15.

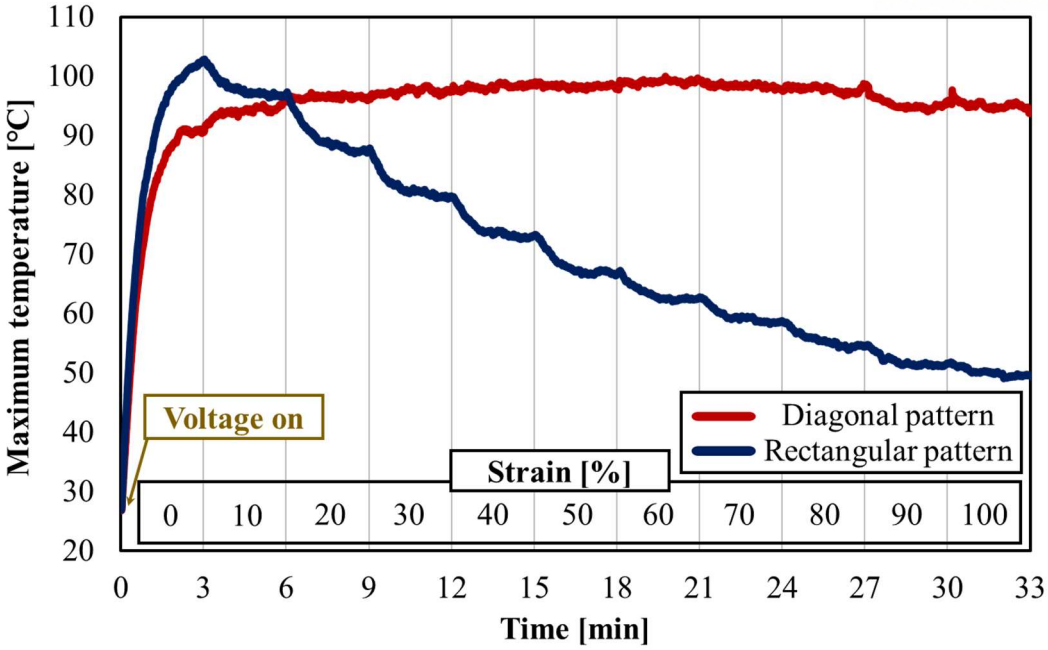

Figure 4.14 Maximum temperature – time curves of the diagonal and rectangular heaters

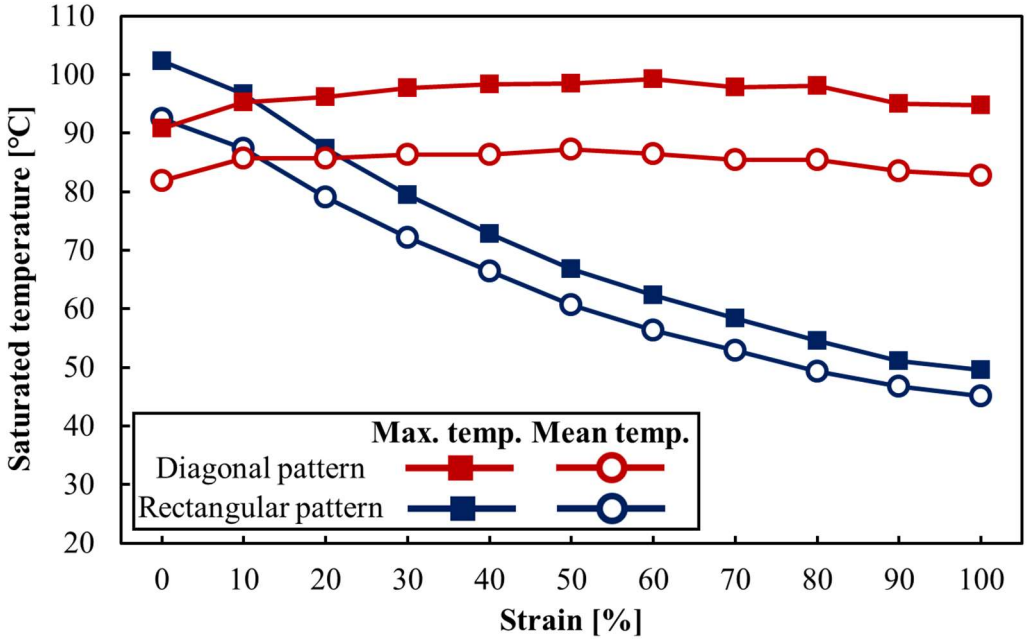

Figure 4.15 Saturated temperature – strain curves of the diagonal and rectangular heaters

The detailed data of the saturated maximum and mean temperatures are presented in Table 4.3. Here, saturated mean temperatures were used as the standard for temperature change by following reasons; 1) in the derivation of the resistance change required for a constant temperature, the temperature on the entire heating area was considered, 2) the saturated heating was considered because the steady-state was assumed, and 3) the maximum temperature could be significantly affected by local deformation,

which is likely triggered by the invasion of defects, such as invisible size fine dust and bubbles, in the elastomer matrix. During the tensile-heating test with the diagonal patterned heater, these defects seemed to affect the dissimilarity in the strain where the biggest maximum and mean temperature occurred (top two yellow boxes in Table 4.3). Based on the saturated mean temperature relative to the initial mean temperature value, the temperature changes in the two heater differed by up to 7.9 times: the biggest temperature changes in the diagonal and rectangular heaters were, respectively, a 6.5% increase at 50% strain and a 51.2% decrease at 100% strain. Thus, it is concluded that a diagonal line is more suitable as the pattern of the wire in the stretchable heater than a tensile directional line, which is commonly adopted in previous studies [27, 29].

Saturated temp. [℃] \ Strain [%]		0	10	20	30	40	50	60	70	80	90	100
Diagonal pattern	Max. temp. (T_{max})	90.8	95.3	96.2	97.7	98.4	98.5	99.2	97.9	98.1	95.1	94.8
	$(T_{max} - T_{max,0})/T_{max,0}$ [%]	0.0	5.0	6.0	7.6	8.4	8.5	9.3 (max.)	7.8	8.0	4.7	4.4
	Mean temp. (T_{mean})	81.9	85.7	85.7	86.3	86.3	87.2	86.5	85.5	85.4	83.5	82.8
	$(T_{mean} - T_{mean,0})/T_{mean,0}$ [%]	0.0	4.6	4.6	5.4	5.4	6.5 (max.)	5.6	4.4	4.3	2.0	1.1
	$T_{max} - T_{mean}$	8.9	9.6	10.5	11.4	12.1	11.3	12.7	12.4	12.7	11.6	12.0
Rectangular pattern	T_{max}	102.3	96.7	87.4	79.5	72.8	66.8	62.4	58.4	54.6	51.2	49.6
	$(T_{max} - T_{max,0})/T_{max,0}$ [%]	0.0	-5.4	-14.5	-22.3	-28.8	-34.7	-39.0	-42.8	-46.6	-50.0	-51.5 (min.)
	T_{mean}	92.5	87.4	79.1	72.2	66.4	60.7	56.3	52.9	49.3	46.8	45.1
	$(T_{mean} - T_{mean,0})/T_{mean,0}$ [%]	0.0	-5.5	-14.5	-21.9	-28.2	-34.4	-39.1	-42.8	-46.7	-49.4	-51.2 (min.)
	$T_{max} - T_{mean}$	9.8	9.3	8.3	7.3	6.4	6.1	6.1	5.5	5.3	4.4	4.5

Table 4.3 Data of saturated temperatures of the diagonal and rectangular heaters

Unfortunately, it is inevitable that the diagonal patterned heater had temperature changes under strain, as suggested by the existence of the extrema gap, which means the result of a difference between the actual and desired resistance change. As shown in Figures 4.8, 4.9 and Table 4.2, the biggest extrema gap of the diagonal heater is 5.9% at 43.5% strain, and these are similar to the measured biggest temperature change of 6.5% at 50% strain (second yellow box from the top in Table 4.3), suggesting that the extrema gap has strong relationship with the temperature change. However, the infrared camera had a measurement error of about ±0.5℃, making the temperature change have errors of up to 1.2%p, and it is supposed to be the reason for the 0.6%p dissimilarity between the biggest extrema gap and the biggest temperature change.

In the meantime, the 6.5%p dissimilarity in the occurrence strain between the biggest extrema gap and the biggest temperature change seemed to be mainly due to the thermal expansion of the elastomer matrix, which made the actual stretch of the heater shorter than the applied strain by the tensile test machine. In other words, the strain range to maintain the heating temperature constant is required to be shorter than the strain range given from the tensile test machine, and thus, the verticality of the diagonal pattern in an eGaIn heater is needed to be smaller than 4. Through the tests with a diagonal heater having a verticality of 3.8 (Figures 4.16, 4.17, and Table 4.4), the smaller verticality was empirically proved to have a fewer temperature change under strain.

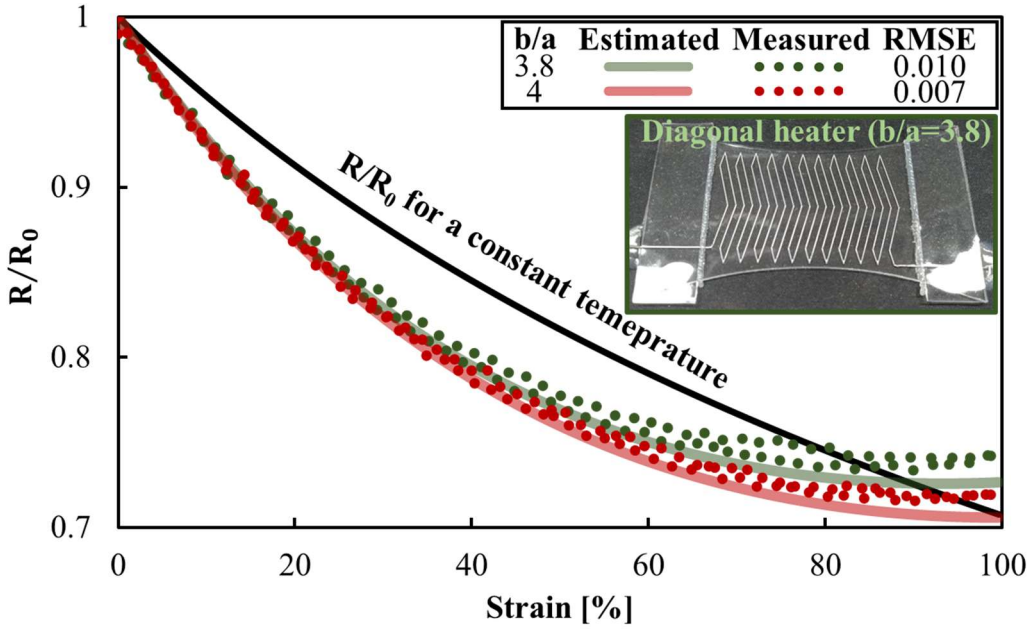

Figure 4.16 Resistance change – strain curves of diagonal heaters with verticalities of 3.8 and 4

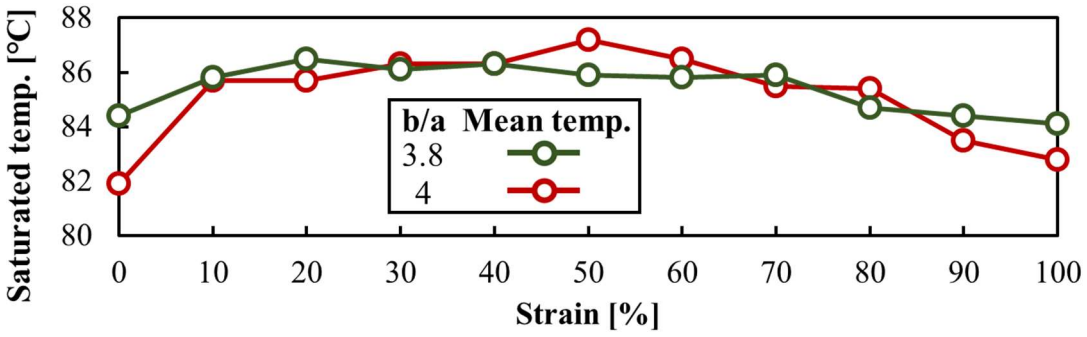

Figure 4.17 Saturated temperature – strain curves of diagonal heaters with verticalities of 3.8 and 4

Saturated temp. [°C] \ Strain [%]		0	10	20	30	40	50	60	70	80	90	100
Diagonal pattern (b/a=3.8)	T_{mean}	84.4	85.8	86.5	86.1	86.3	85.9	85.8	85.9	84.7	84.4	84.1
	$(T_{mean} - T_{mean,0})/T_{mean,0}$ [%]	0.0	1.7	2.5 (max.)	2.0	2.3	1.8	1.7	1.8	0.4	0.0	-0.4
Diagonal pattern (b/a=4)	T_{mean}	81.9	85.7	85.7	86.3	86.3	87.2	86.5	85.5	85.4	83.5	82.8
	$(T_{mean} - T_{mean,0})/T_{mean,0}$ [%]	0.0	4.6	4.6	5.4	5.4	6.5 (max.)	5.6	4.4	4.3	2.0	1.1

Table 4.4 Data of saturated temperatures of the diagonal heaters

Although the temperature change of less than 3% in a strain range of 0~100% was realized with a diagonal patterned eGaIn heater of a 3.8 verticality, two issues still remain. First is the increased difference in the maximum and mean temperatures of the diagonal heater under strain (Table 4.3). The difference in the maximum and mean temperatures is important because it plays a role as an indicator of the non-uniformity in heating. Referring to Figure 4.10, it can be easily guessed that the intervals between the diagonal patterned wires became more distant under strain, resulting in the increased non-uniformity, while the intervals between the rectangular patterned wires became narrower. Hence, a way for patterning the diagonal lines is demanded to be modified for a decreased non-uniformity under strain, for example, as shown in Figure 4.18. In this thesis, the temperature change under strain has been a major concern, so the method for a decreased non-uniformity in heating remains an open issue.

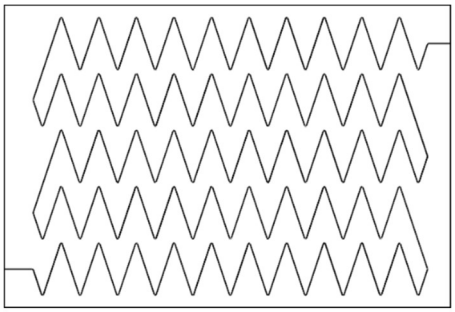

Figure 4.18 An example of a diagonal pattern to keep a heating uniformity under strain

Another issue is that the thermal expansion of the elastomer matrix has not been investigated. Due to no investigation on any thermal effects, the verticality of 3.8 was randomly decided but fortunately, the diagonal heater with it had a further smaller temperature change than a diagonal pattern with a verticality of 4. To design an eGaIn wire trajectory for a smaller temperature change under strain, examination of the thermal effects such as thermal expansion also remains an open issue.

4.2.4 Comparison with other study

The realization of the temperature change of less than 3% in a strain range of 0~100% by only patterning the eGaIn wire is a noteworthy achievement when compared with other stretchable heaters. In existing studies on stretchable heaters, a mixture of different materials has been used as an electrical wire in a heater [25, 28, 29], but as various materials needed to be prepared and mixed, it has been difficult to fabricate heaters. Meanwhile, the stretchable heaters proposed in this thesis have used only eGaIn as electrical wires, which naturally led to simple fabrication. In addition to the simple fabrication, the heaters in this thesis demonstrated enormously small changes in temperature (less than 3%) even in a high tensile condition (100% strain). Comparing to stretchable heaters in other studies which have specified temperature changes under strain [20, 59-70], it can be proved how well the heater introduced in this thesis maintained the heating temperature even at high strain (Figure 4.19 and Table 4.5).

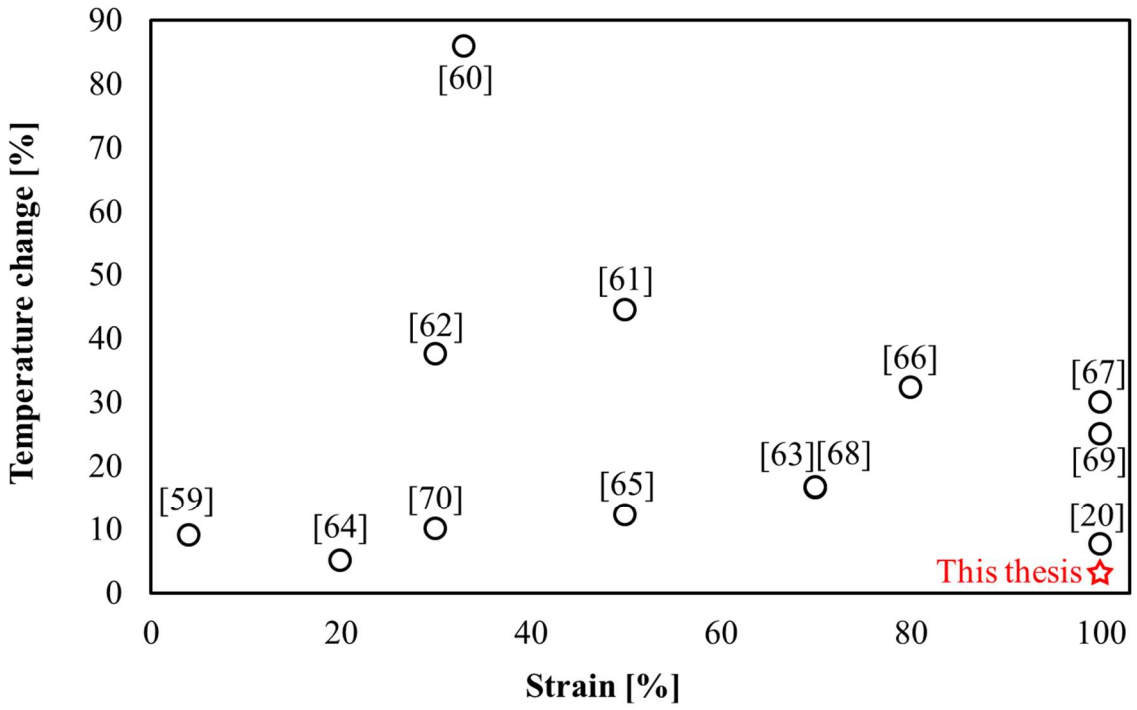

Figure 4.19 Comparison to other stretchable heaters [20, 59-70]

Ref.	[59]	[60]	[61]	[62]	[63]	[64]	[65]	[66]	[67]	[20]	[68]	[69]	[70]	This thesis
Temp. change	9%	85.9%	44.4%	37.5%	16.6%	5%	12.2%	32.3%	30%	7.6%	16.7%	25%	10%	2.9%
Strain range	4%	33%	50%	30%	70%	20%	50%	80%	100%	100%	70%	100%	30%	100%
Material for wire	Graphene	Graphene	Copper nanowires	Silver nanowires	Carbon-ized fabric	Silver film	Silver nanowires	Copper nanowires	Carbon-nanotubes	Mixture (PDMS + liquid metal)	Carbon-ized fabric	Carbon-nanotubes	Ionomers	eGaIn

Table 4.5 Data of comparison to other stretchable heaters [20, 59-70]

4.3 eGaIn patterning for minimized resistance changes under strain

4.3.1 Design of eGaIn patterns for minimization of resistance changes under strain

In Chapter 4.2, resistance was adjusted to be decreased under strain. On the other hand, some studies have attempted to develop eGaIn wires with no change in their resistance under strain for connection among electronic components like a resistor, light-emitting diode, amplifier, and microcontroller [35, 71-73]. Although some studies have introduced stretchable wires with impressively small resistance changes under the strain of over 500 % by using the mixtures of eGaIn and solid conductors [72, 73], their considerations were on only the materials but no design of wire trajectories. Here, the resistance estimation models present the adjustability of resistance changes, which suggests that eGaIn pattering can help eliminate changes in resistance. For instance, eGaIn wires patterned by combined two arcs have a possibility to achieve minimized resistance changes under strain by adjusting the length ratio or ending angles of the two arcs. Figure 4.20 presents the estimated resistance changes in the eGaIn wires patterned by combined two arcs under strain with regard to the $arc_{45°\&90°}$, which is defined as a length ratio of two arc wires with the same starting angles of 0° and different ending angles of 45° and 90°.

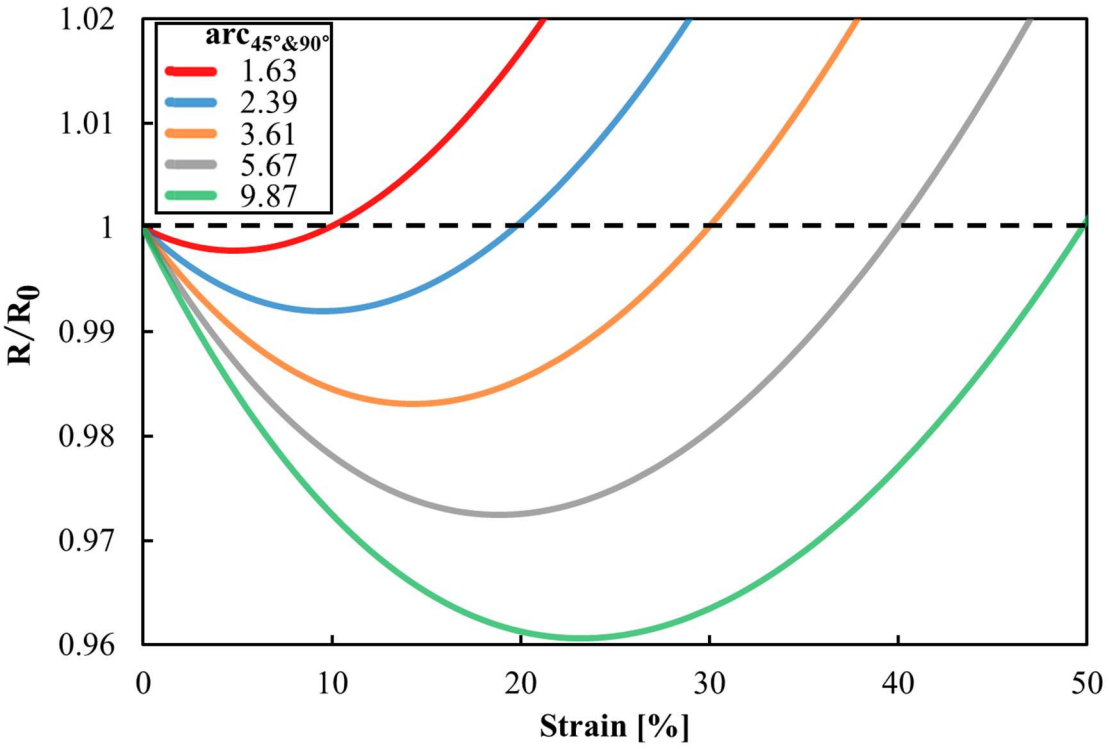

Figure 4.20 Estimated resistance changes in combined two arc eGaIn wires

As a first step to select eGaIn wire patterns to minimize resistance changes under strain, “the resistance breadth” is defined as the difference between the maximum and minimum values of resistance in a specific strain range. Here, if the strain range is set from 0% to the strain where the resistance becomes the second initial resistance value, the resistance breadth becomes minimized within a maximized strain range, as shown in Figure 4.21 and Table 4.6.

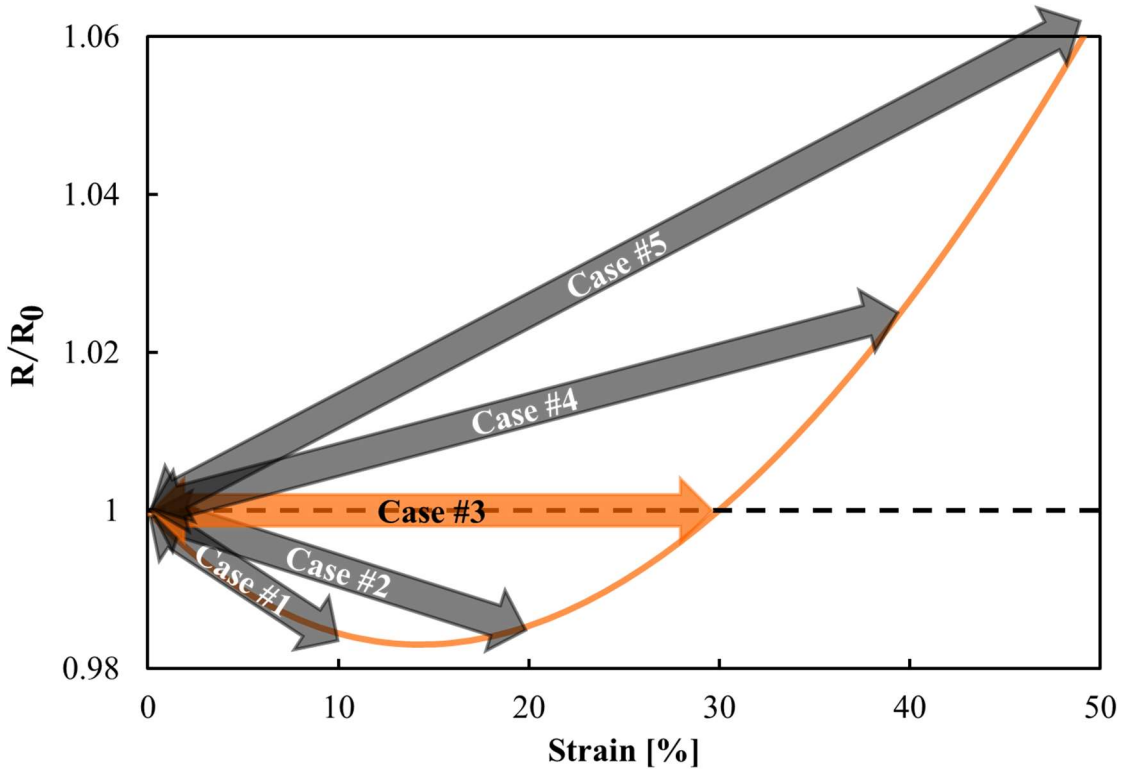

Figure 4.21 A resistance change in combined two arcs with an $arc_{45°\&90°}$ of 3.61

Case	#1	#2	#3	#4	#5
Strain range setting	0% ~ 10%	0% ~ 20%	0% ~ 30%	0% ~ 40%	0% ~ 50%
Max. resistance change $(R/R_0)_{max}$ [%]	100	100	100	102.67	106.37
Min. resistance change $(R/R_0)_{min}$ [%]	98.45	98.31	98.31	98.31	98.31
Resistance breadth [%]	**1.55**	**1.69**	**1.69**	**4.36**	**8.06**

Table 4.6 Resistance breadths of two arcs with an $arc_{45°\&90°}$ of 3.61 according to strain ranges

The resistance breadth becomes bigger when a wider strain range is targeted by adjusting the length ratio as shown in Figure 4.22, and in this thesis, the resistance breadths were targeted to be less than 5%.

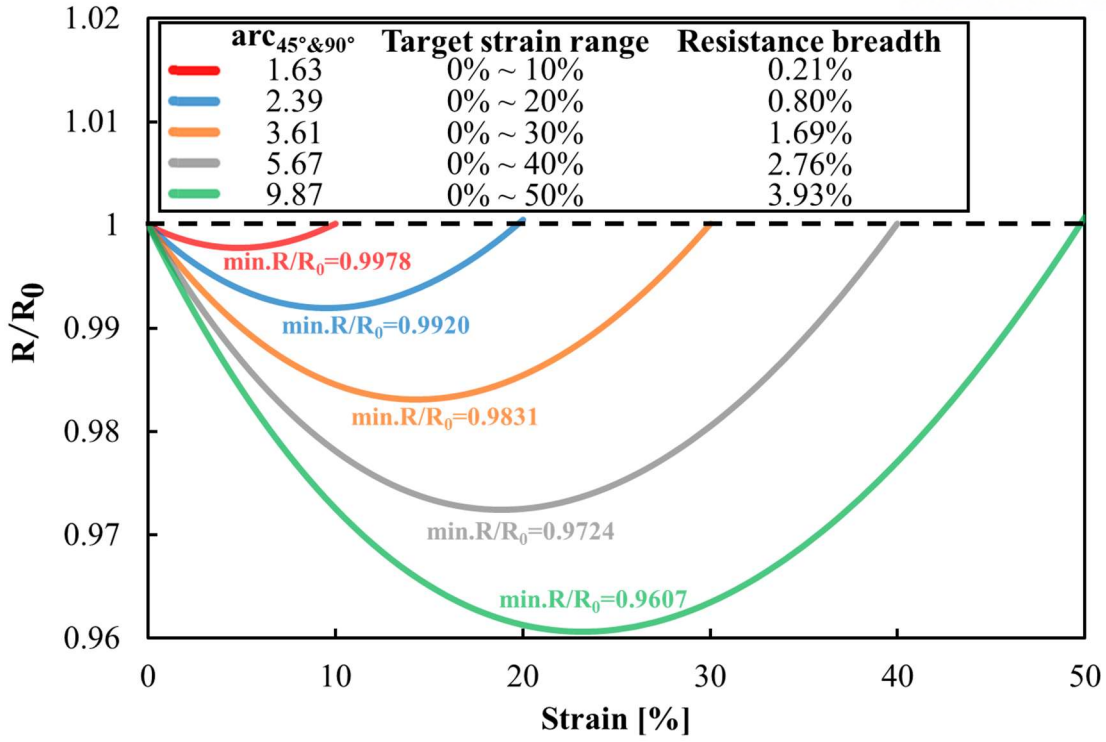

Figure 4.22 Resistance changes in combined two arcs with various $arc_{45°\&90°}$s

4.3.2 Fabrication of patterned eGaIn wires

To minimize resistance changes in strain ranges of 0~30% and 0~50%, samples were fabricated by patterning eGaIn wires on the basis of combined two arcs with an $arc_{50°\&90°}$ of 7.60 and $arc_{45°\&90°}$ of 9.87. The fabrication method was the same as aforementioned, and the fabricated samples are presented in Figure 4.23.

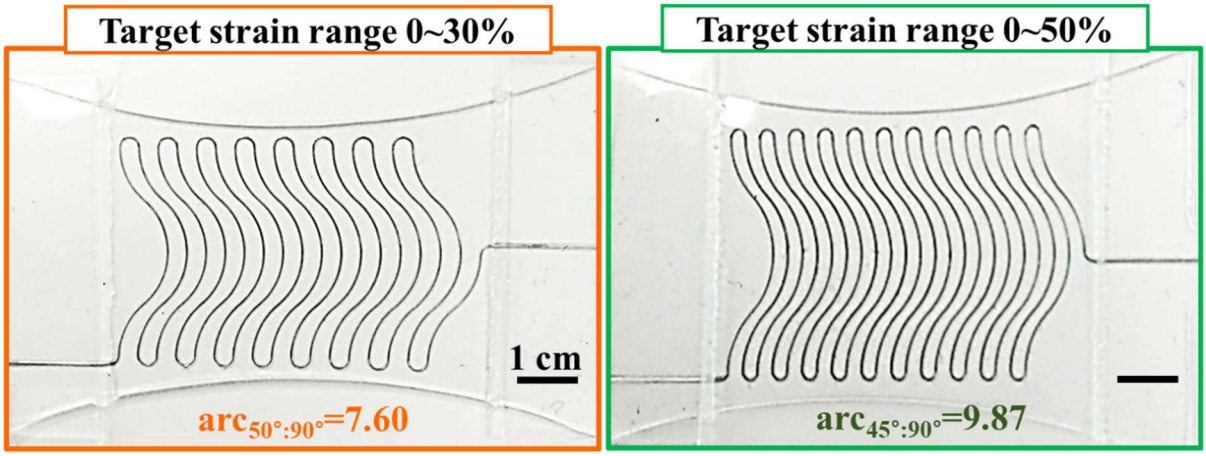

Figure 4.23 The fabricated samples for minimized changes in their resistance

4.3.3 Tensile test results

The fabricated samples were elongated within the respective targeted strain range in the same way as aforementioned except for a strain rate of 0.5mm/s, and the measured resistance changes in the two samples were compared to the resistance changes estimated by the estimation model for a circular arc-shaped eGaIn wire. As shown in Figure 4.24, the estimated and measured resistance changes were extremely similar to each other in both samples with estimation errors of less than 0.003. These errors could be small because the resistance changes themselves were small and lengths of arc-patterned eGaIn wires in the samples were long, taking up about 97% of the total wire lengths, which results in the reduction in the effects of the copper wire insertion. Figure 4.24 also demonstrates that resistance changes of 2.2% and 4.6% in the strain ranges of 0~30% and 0~50%, respectively, could be realized by patterning arc eGaIn wires.

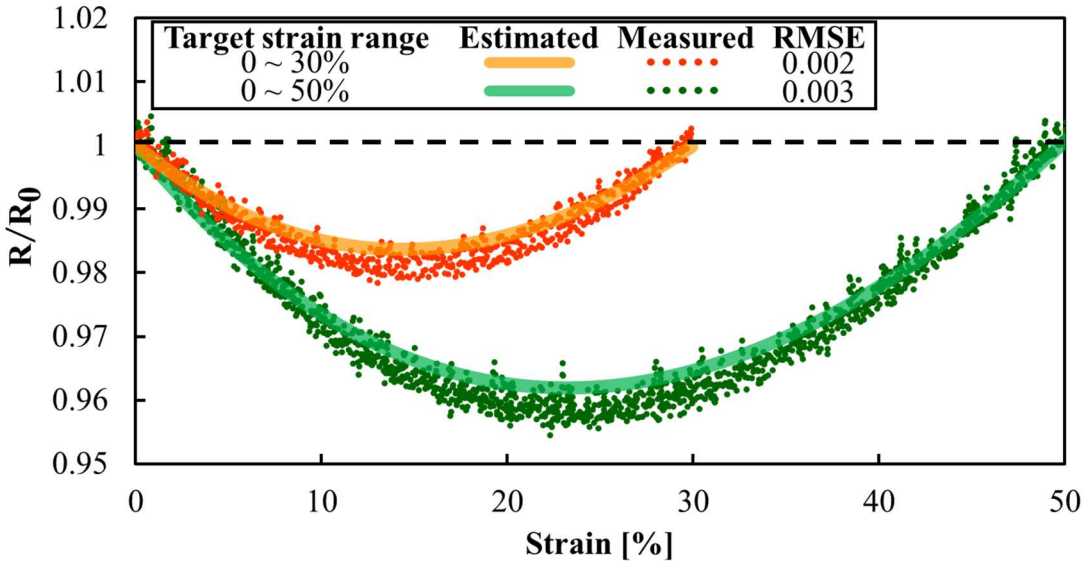

Figure 4.24 The estimated and measured resistance changes in the two samples

Even if the estimation errors were much small, the measured resistance changes were 0.5%p and 0.7%p bigger than the estimated resistance changes in the two sample (Table 4.7). The hysteresis was guessed to have little effect on the errors due to a strain rate ten times slower than that in the cases of the aforementioned samples. It seems that the non-iso-volumetry mentioned in Chapter 3.3.2 was the main cause of the errors, in that the non-iso-volumetry is linked to the volume increase under strain so makes the actual resistance values smaller than the estimated values through the assumption of the iso-volumetry. However, the degree of the non-iso-volumetry was not that great so was slightly affected the errors. As a result, eGaIn wires with resistance changes of less than 5% in a strain range of 0~50% could be proposed, and the eGaIn patterning is proved to have its usefulness for eGaIn-based applications requiring no resistance changes under strain.

Target strain range	Estimated min. resistance change	Measured min. resistance change	Estimated resistance breadth	Actual Resistance breadth
0 ~ 30%	0.9836	0.9781	**1.64%**	**2.19%**
0 ~ 50 %	0.9618	0.9544	**3.82%**	**4.56%**

Table 4.7 The estimated and actual resistance breadths

4.3.4 Comparison with other study

Although the eGaIn wires proposed in this thesis have relatively high resistance changes under low strain compared to other studies (Figure 4.25) [72, 73], the resistance estimation models can be applied to the other studies, in which the wires were placed in the tensile direction, to further reduce changes in resistance of their wires. The reduction in resistance changes through eGaIn patterning fundamentally results from switching wire deformation that makes resistance changes into wire rotation that makes no resistance change, therefore, much smaller resistance changes are expected when the resistance estimation models are used for patterning eGaIn-based mixtures introduced in other studies.

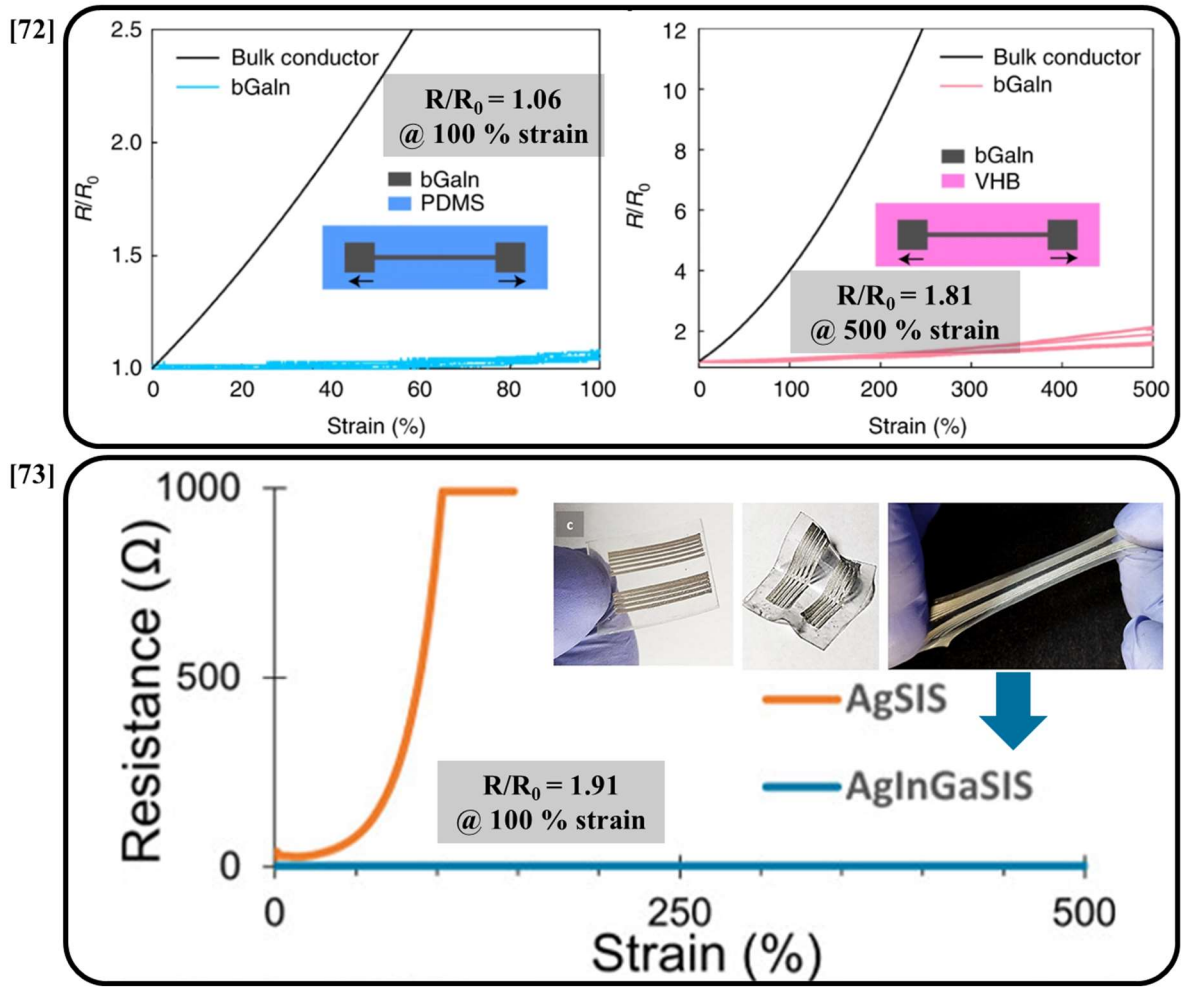

Figure 4.25 Tensile directional eGaIn-based wires in existing studies [72, 73]

Chapter 5. Conclusion and open issues

In this thesis, resistance changes in diagonal and circular arc-shaped eGaIn wires under strain were formulated with the assumption that deformation of eGaIn wires under strain is dominated by the iso-volumetric elastomer matrix. The derived resistance estimation models suggest that the resistance changes in the diagonal and circular arc-shaped eGaIn wires under strain can be adjusted depending on the initial tilt angle of the diagonal eGaIn wire and the initial starting or ending angle of the circular arc-shaped eGaIn wire, respectively. Samples of eGaIn wires patterned by diagonal lines and circular arcs were fabricated and elongated up to 150% strain to experimentally verify the models. Tensile test results proved that resistance values estimated by the models were extremely similar to the measured resistance values with estimation errors (root mean square errors) of less than 0.05. The errors seemed to be mainly caused by variance in copper wire insertions during sample fabrication.

With the verified models, the resistance change under strain was estimated in an eGaIn strain sensor that includes semicircular wires, and inspected by tensile tests with a strain range of 0~150%. Under strain, the resistance values estimated with consideration of the semicircular wire were more similar to the measured resistance values with a 56.07% decrease in estimation error, compared to the resistance values estimated without considered semicircular wire. Also, the model was used for patterning eGaIn wires of a stretchable heater, whose temperature is needed to be constant under strain. The resistance change required for the constant heating temperature in a strain range of 0~100% was examined, and approximately realized by fabricating eGaIn heaters which have wires patterned by diagonal lines with verticalities (tangent of tilt angles) of 3.8 and 4. Through the heating tests, the eGaIn heaters were proved to have temperature changes of less than 7% in a strain range of 0~100%. Lastly, the model was applied for patterning eGaIn wires which have minimized resistance changes under strain. The minimized resistance changes of combined two arc wires were examined in a strain range of 0~50%, and approximately realized by fabricating samples that have wires of the combined two arcs with different ending angles and length ratios. Through the tensile tests, the eGaIn wires were proved to have resistance changes of less than 5% in a strain range of 0~50%. In conclusion, the resistance estimation models proposed in this thesis are expected to help in the estimation of resistance changes and the design of wire trajectories for eGaIn-based stretchable electronics.

Although this thesis considered only utilization of the estimation models, the estimation models also have expandability; 1) the resistance changes under compressive strain can be formulated in the same way as the aforementioned models were derived, if the internal compressive stress is uniform in the whole of cross-sections. For example, the estimation model for the compressive strain is applicable to pressure sensors having cross-sections where eGaIn wires account for most of the area. 2) The estimation model for diagonal eGaIn wires can be extended from two-dimensions to three-dimensions. In this thesis, only eGaIn wires on a two-dimensional plane were considered, but it is also enable to

derive resistance changes in three-dimensional eGaIn wires under strain using equation (2.5), which means that the resistance changes are equal to the square of length changes. 3) Additionally, resistance changes in sinusoidal and oval patterned eGaIn wires under strain can be derived through equation (2.5).

Moreover, if the thermal expansion of the eGaIn heater is examined and considered when designing the eGaIn trajectory, the heater may have even constant temperatures under strain than proposed in Chapter 4.2. Plus, if the eGaIn wires are fabricated with eGaIn-mixtures as shown in existing studies [72, 73] and patterned by diagonal lines or arcs, they are expected to have much fewer resistance changes under strain than proposed in Chapter 4.3.

References

[1] MarketandMarkets Research Private Ltd. (2019, November). Industrial Wearable Market by Device Type (AR Glasses, VR Headsets, Smartwatches, Smart Bands), Industry (Automotive, Aerospace, Manufacturing, Oil & Gas, Power & Energy), Component, and Region – Global Forecast to 2024. Retrieved from https://www.marketsandmarkets.com/Market-Reports/industrial-wearable-market-240394537.html

[2] IDTechEx Ltd. (2017, August). Wearable Technology 2017-2027: Markets, Players, Forecasts. Retrieved from https://www.idtechex.com/en/research-report/wearable-technology-2017-2027-markets-players-forecasts/536

[3] Wang, X., Li, J., Song, H., Huang, H., & Gou, J. (2018, February). Highly Stretchable and Wearable Strain Sensor Based on Printable Carbon Nanotube Layers/Polydimethylsiloxane Composites with Adjustable Sensitivity. *ACS Applied Materials and Interfaces*, 10(8), 7371-7380.

[4] Kim, H., Yarin, A. L., & Lee, M. W. (2019, October). Ultra-fast bull's eye-like self-healing using CNT heater. *Polymer*, 180, 121710.

[5] Bengio, E. A., Senic, D., Taylor, L. W., Tsentalovich, D. E., Chen, P., Holloway, C. L., … & Pasquali, M. (2017, June). High efficiency carbon nanotube thread antennas. *Applied Physics Letters*, 111, 163109.

[6] Kim, M., Kim, M., Kwon, H., Jo, S., & Kim, Y. (2017, October). Wearable triboelectric nanogenerator using a plasma-etched PDMS–CNT composite for a physical activity sensor. *RSC Advances*, 7, 48368-48373.

[7] Kim, S., Kim, J., & Park, J. (2017, July). Wearable and Transparent Capacitive Strain Sensor with High Sensitivity Based on Patterned Ag Nanowire Networks. *ACS Applied Materials and Interfaces*, 9(31), 26407-26416.

[8] Huang, Q., Al-Milaji, K. N., & Zhao, H. (2018, August). Inkjet Printing of Silver Nanowires for Stretchable Heaters. *ACS Applied Nano Materials*, 1(9), 4528-4536.

[9] Min, K., Umar, M., Seob, H., Yim, J. H., Kam, D. G., Jeon, H., … & Kim, S. (2017, January). Biocompatible, optically transparent, patterned, and flexible electrodes and radio-frequency antennas prepared from silk protein and silver nanowire networks. *RSC Advances*, 7, 574-580.

[10] Zhou, Q., Kim, J., Han, K., Oh, S., Umrao, S., Chae, E. J., & Oh. I. (2019, May). Integrated dielectric-electrode layer for triboelectric nanogenerator based on Cu nanowire-Mesh hybrid electrode. *Nano Energy*, 59, 120-128.

[11] Wang, X., Guo, R., Yuan, B., Yao, Y., Wang, F., & Liu, J. (2018, July). Ni-doped Liquid Metal Printed Highly Stretchable and Conformable Strain Sensor for Multifunctional Human-Motion Monitoring. In 2018 40th Annual International Conference of the IEEE Engineering in Medicine and Biology Society (EMBC) (pp. 3276-3279). IEEE.

[12] Guo, R., Wang, H., Sun, X., Yao, S., Chang, H., Wang, H., … & Zhang, Y. (2019, July). Semiliquid Metal Enabled Highly Conductive Wearable Electronics for Smart Fabrics. *ACS Applied Materials and Interfaces*, 11(33), 30019-30027.

[13] Hayes, G. J., So, J., Qusba, A., Dickey, M. D. & Lazzi, G. (2012, April). Flexible Liquid Metal Alloy (EGaIn) Microstrip Patch Antenna. *IEEE Transactions on Antennas and Propagation*, 60(5), 2151-2156.

[14] Yang, Y., Sun, N., Wen, Z., Cheng, P., Zheng, H., Shao, H., … & Lee, S. (2018, February). Liquid-Metal-Based Super-Stretchable and Structure-Designable Triboelectric Nanogenerator for Wearable Electronics. *ACS Nano*, 12(2), 2027-2034.

[15] Dickey, M. D. (2017, April). Stretchable and soft electronics using liquid metals. *Advanced Materials*, 29(27), 1606425.

[16] Chiechi, R. C., Weiss, E. A., Dickey, M. D., & Whitesides, G. M. (2007, December). Eutectic Gallium-Indium (eGaIn): A moldable liquid metal for electrical characterization of self-assembled monolayers. *Angewandte Chemie International Edition*, 47(1), 142-144.

[17] Dickey, M. D. (2014, October). Emerging applications of liquid metals featuring surface oxides. *ACS Applied Materials and Interfaces*, 6(21), 18369-18379.

[18] Kim, S., Oh, J., Jeong, D., Park, W. & Bae, J. (2018, October). Consistent and reproducible direct ink writing of eutectic Gallium-Indium for high-quality soft sensors. *Soft Robotics*, 5(5), 601-612.

[19] Ogden, R. W. (1984). Non-linear Elastic Deformations. Chichester: Ellis Harwood Ltd.

[20] Kim, S., Lee, J., & Choi, B. (2015, July). Stretching and sensing with liquid-metal strain gauges printed on silicone elastomers. *IEEE Sensors Journal*, 15(11), 6077-6078.

[21] Chen, J., Zhu, Y., & Jiang, W. (2020, January). A stretchable and transparent strain sensor based on sandwich-like PDMS/CNTs/PDMS composite containing an ultrathin conductive CNT layer. *Composites Science and Technology*, 186, 107938.

[22] Zhao, M., Li, D., Huang, J., Wang, D., Mensah, A., & Wei, Q. (2019, October). A multifunctional and highly stretchable electronic device based on silver nanowire/wrap yarn composite for a wearable strain sensor and heater. *Journal of Materials Chemistry C* , 7, 13468–13476.

[23] Chen, J., Zhang, J., Luo, Z., Zhang, H., Li, L., Su, Y., … & Li, H. (2020, April). Superelastic, sensitive, and low hysteresis flexible strain sensor based on wave-patterned liquid metal for human activity monitoring. *ACS Applied Materials and Interfaces*, 12(19), 22200-22211.

[24] White, E. L., Case, J. C., & Kramer, R. K. (2017, January). Multi-mode strain and curvature sensors for soft robotic applications. *Sensors and Actuators A: Physical*, 253, 188-197.

[25] Jo, H. S., An, S., Lee, J., Park, H. G., Al-deyab, S., Yarin, A. L., and Yoon, S. S. (2017, February). Highly flexible, stretchable, patternable, transparent copper fiber heater on a complex 3D surface. *NPG Asia Materials,* 9, e347.

[26] Oh, J., Kim, S., Lee, S., Jeong, S., Ko, S. H. and Bae, J. (2020, December). A liquid metal based multimodal sensor and haptic feedback device for thermal and tactile sensation generation in virtual reality. *Advanced Functional Materials*, 2007772.

[27] Li, Y., Feng, S., Cao, S., Zhang, J., & Kong, D. (2020, October). Printable liquid metal microparticle ink for ultrastretchable electronics. *ACS Applied Materials and Interfaces*, 12(45), 50852-50859.

[28] Sohn, Y., & Chu, K. (2020, April). Flexible hybrid conductor comprising eutectic Ga-In liquid metal and Ag nanowires for the application of electronic skin. *Materials Letters*, 265, 127223.

[29] Tavakoli, M., Malakooti, M. H., Paisana, H., Ohm, Y., Marques, D. G., Lopes, P. A., … & Majidi, C. (2018, May). eGaIn-assisted room-temperature sintering of silver nanoparticles for stretchable, inkjet-printed, thin-film electronics. *Advanced Materials*, 30(29), 1801852.

[30] Michaud, H. O., Reixidor, J., & Lacour, S. P. (2015, February). Soft metal constructs for large strain sensor membrane. *Smart Materials and Structures*, 24(3), 035020.

[31] Privat-Deschanel, A., (1874). Elementary Treatise on Natural Philosophy: Electricity and magnetism. New York: D. Appleton and Company.

[32] Wolf, F. P. (1972, July). Elastic behaviour of rubber under small uniaxial extension and compression. *Polymer*, 13(7), 347-354.

[33] Pineda, F., Bottausci, F., Icard, B., Malaquin, L., & Fouillet, Y. (2015, August). Using electrofluidic devices as hyper-elastic strain sensors: Experimental and theoretical analysis. *Microelectronic Engineering*, 144, 27-31.

[34] Wang, Y., Yu, Z., Mao, G., Liu, Y., Liu, G., Shang, J., … & Li, R. (2018, November). Printable Liquid-Metal@PDMS Stretchable Heater with High Stretchability and Dynamic Stability for Wearable Thermotherapy. *Advanced Materials Technologies*, 4(2), 1800435.

[35] Yoon, J., Hong, S. Y., Lim, Y., Lee, S., Zi, G., & Ha, J. S. (2014, August). Design and Fabrication of Novel Stretchable Device Arrays on a Deformable Polymer Substrate with Embedded Liquid-Metal Interconnections. *Advanced Materials*, 26(38), 6580-6586.

[36] Sigma-Aldrich. (2019). *Gallium-Indium eutectic*. [Material]. https://www.sigmaaldrich.com/

[37] Smooth-On. (2019). *Solaris™*. [Material]. https://www.smooth-on.com/

[38] Eduntech. (2019). *Micrometer film applicator*. [Apparatus]. Bucheon, Kyonggi-do, Korea.

[39] Hanbaek science. (2015). *Drying oven* (HB-501M). [Equipment]. https://www.hanbaeksci.co.kr/

[40] Musashi Engineering. (2020). *Desktop robot* (SHOTMASTER300ΩX). [Equipment]. http://www.musashi-engineering.co.jp.e.cn.hp.transer.com/

[41] Swann-Morton. (2020). *Number 4 Handle*. [Apparatus]. https://www.swann-morton.com/

[42] Swann-Morton. (2020). *Number 25A Blade*. [Apparatus]. https://www.swann-morton.com/

[43] Shin-Etsu Chemical. (2018). *X-32-949T*. [Material]. https://www.shinetsu.co.jp/en/

[44] Kim, D., Lee, Y., Lee, D., Choi, W., Yoo, K., & Lee, J. (2015, February). Hydrochloric acid-impregnated paper for gallium-based liquid metal microfluidics. *Sensors and Actuators B: Chemical*, 207(A), 199-205.

[45] Musashi Engineering. (2018). *Nozzle & needle* (TPND-22G-U). [Apparatus]. http://www.musashi-engineering.co.jp.e.cn.hp.transer.com/

[46] AnMo Electronics. (2020). *Dino-lite* (AM4013MT). [Apparatus]. http://www.dino-lite.com/

[47] MIDAS Information Technology. (2020). *MeshFree 2020*. [Software] https://www.midasuser.com/

[48] Kim, T. K., Kim, J. K., & Jeong, O. C. (2011, August). Measurement of nonlinear mechanical properties of PDMS elastomer. *Microelectronics Engineering*, 88(8), 1982-1985.

[49] Dongbu Robot. (2013). *Desktop Robot* (DTR3-3310). [Equipment]. http://www.hyulimrobot.com/

[50] Omron. (2019). *Displacement Sensors / Measurement Sensors* (ZX1-LD300A61). [Equipment]. http://www.ia.omron.com/

[51] National Instruments. (2017). *Multifunction I/O* (USB-6351). [Equipment]. https://www.ni.com/

[52] National Instruments. (2020). *LabVIEW 2020*. [Software]. https://www.ni.com/

[53] Autodesk. (2019). *AutoCAD 2019*. [Software]. https://www.autodesk.com/

[54] Mott, P. H., & Roland, C. M. (2012, April). Limits to Poisson's ratio in isotropic materials – general

result for arbitrary deformation. *Physica Scripta*, 87(5), 055404.

[55] Steck, D., Qu, J., Kordmahale, S. B., Tscharnuter, D., Muliana, A., & Kameoka, J. (2018, August). Mechanical responses of Ecoflex silicone rubber: Compressible and incompressible behaviors. *Journal of Applied Polymer Science*, 136(5), 47025.

[56] Oliveri, A., Maselli, M., Lodi, M., Storace, M., & Cianchetti, M. (2019, October). Model-Based Compensation of Rate-Dependent Hysteresis in a Piezoresistive Strain Sensor. *IEEE Transactions on Industrial Electronics*, 66(10), 8205-8213.

[57] ODA Technologies. (2017). *Programmable DC Power Supply* (OPE-305QI). [Equipment]. https://www.odacore.com/main/

[58] FLIR Systems. (2018). *Thermal Imaging Camera* (C3). [Equipment]. https://www.flir.com/

[59] Kang, J., Kim, H., Kim, K. S., Lee, S., Bae, S., Ahn, J., … & Hong, B. H. (2011, November). High-Performance Graphene-Based Transparent Flexible Heaters. *Nano Letters*, 11(12), 5154-5158.

[60] Wang, R., Xu, Z., Zhuang, J., Liu, Z., Peng, L., Li, Z., … & Gao, C. (2016, December). Highly Stretchable Graphene Fibers with Ultrafast Electrothermal Response for Low-Voltage Wearable Heaters. *Advanced Electronic Materials*, 3(2), 1600425

[61] Ding, S., Jiu, J., Gao, Y., Tian, Y., Araki, T., Sugahara, T., … & Uchida, H. (2016, February). One-Step Fabrication of Stretchable Copper Nanowire Conductors by a Fast Photonic Sintering Technique and Its Application in Wearable Devices. *Applied Materials and Interfaces*, 8(9), 6190-6199.

[62] Hong, S., Lee, H., Lee, J., Kwon, J., Han, S., Suh, Y. D., … & Ko, S. H. (2015, July). Highly Stretchable and Transparent Metal Nanowire Heater for Wearable Electronics Applications. *Advanced Materials*, 27(32), 4744-4751.

[63] Zhang, M., Wang, C., Liang, X., Yin, Z., Xia, K., Wang, H., … & Zhang, Y. (2017, August). Weft-Knitted Fabric for a Highly Stretchable and Low-Voltage Wearable Heater. *Advanced Electronic Materials*, 3(9), 1700193.

[64] Ko, E., Kim, H., Lee, S., Kim T., & Kim, H. (2017, April). Stretchable Ag electrodes with mechanically tunable optical transmittance on wavy-patterned PDMS substrates. *Scientific Reports*, 7, 46739.

[65] Choi, S., Park, J., Hyun, W., Kim, J., Kim, J., Lee, Y. B., … & Kim, D. (2015, May). Stretchable Heater Using Ligand-Exchanged Silver Nanowire Nanocomposite for Wearable Articular Thermotherapy. *ACS Nano*, 9(6), 6626-6633.

[66] Cheng, Y., Zhang, H., Wang, R., Wang, X., Zhai, H., Wang, T., … & Sun, J. (2016, September).

Highly Stretchable and Conductive Copper Nanowire Based Fibers with Hierarchical Structure for Wearable Heaters. *ACS Applied Materials and Interfaces*, 8(48), 32925-32933.

[67] Li, Y., Zhang, Z., Li, X., Zhang, J., Lou, H., Shi, X., … & Peng, H. (2016, December). A smart, stretchable resistive heater textile. *Journal of Materials Chemistry C*, 5, 41-46.

[68] Wang, C., Zhang, M., Xia, K., Gong, X., Wang, H., Yin, Z., … & Zhang, Y. (2017, March). Intrinsically Stretchable and Conductive Textile by a Scalable Process for Elastic Wearable Electronics. *Applied materials and Interfaces*, 9(15), 13331-13338.

[69] Lee, Y., Le, V. T., Kim, J., Kang, H., Kim, E. S., Ahn, S., & Suh, D. (2018, January). Versatile, High-Power, Flexible, Stretchable Carbon Nanotube Sheet Heating Elements Tolerant to Mechanical Damage and Severe Deformation. *Advanced Functional Materials*, 28(8), 1706007.

[70] Zhou, R., Li, P., Fan, Z., Du, D., & Ouyang, J. (2017, January). Stretchable heaters with composites of an intrinsically conductive polymer, reduced graphene oxide and an elastomer for wearable thermotherapy. *Journal of Materials Chemistry C*, 5, 1544-1551.

[71] Guo, R., Wang, X., Yu, W., Tang, J., & Liu, J. (2018, May). A highly conductive and stretchable wearable liquid metal electronic skin for long-term conformable health monitoring. *Science China Technological Sciences*, 61, 1031-1037.

[72] Liu, S., Shah, D. S., & Kramer, R. K. (in press). Highly stretchable multilayer electronic circuits using biphasic gallium-indium. *Nature Materials*. Retrieved from https://doi.org/10.1038/s41563-021-00921-8

[73] Lopes, P. A., Fernandes, D. F., Silva, A. F., Marques, D. G., Almeida, A. T., Majidi, C., & Tavakoli, M. (2021, March). Bi-Phasic Ag–In–Ga-Embedded Elastomer Inks for Digitally Printed, Ultra-Stretchable, Multi-layer Electronics. *ACS Applied Materials and Interfaces*, 13(12), 14552-14561.

Acknowledgements

First of all, I would like to thank prof. Joonbum Bae, my advisor. His guidance was a GPS that lights the destination, and has made my master's degree fruitful. I express my respect and appreciation for giving an abundant research environment. I think it was lucky to meet my advisor who had a lot to learn.

I also thank my laboratory colleagues. My research could not be advanced unless they have filled my shortcomings and motivated me to carry on. I will always have gratitude for what they have given me, and I wish them all the best in the future.

Above all, the careful concern and warmth from Dongyoung Lee, Hojae Lee, Hyungju Choi, Hail An, Dongman Lee, Dawon Ju, and Kyeongtaek Kim became a lubricant for my research.

Especially, I will not forget sincere advice and helps from Wookeun Park, Bokwon Kwak, Jeongsoon Hong, and Jihye Oh. Their supports became a compass to get out of the woods. It was an honor to be with them.

Lastly, I give my AROHA to my parents, elder sister, and kinfolks. Their affectionate attention became the fuel to move forward, and nothing could have been done without their mental support. I will continue to work hard to be their pride.